JGP Journal of General Physiology

ARTICLE

ML277 regulates KCNQ1 single-channel amplitudes and kinetics, modified by voltage sensor state

Jodene Eldstrom, Donald A. McAfee, Ying Dou, Yundi Wang, and David Fedida

KCNQ1 is a pore-forming K^+ channel subunit critically important to cardiac repolarization at high heart rates. (2R)-*N*-[4-(4-methoxyphenyl)-2-thiazolyl]-1-[(4-methylphenyl)sulfonyl]-2 piperidinecarboxamide, or ML277, is an activator of this channel that rescues function of pathophysiologically important mutant channel complexes in human induced pluripotent stem cell–derived cardiomyocytes, and that therefore may have therapeutic potential. Here we extend our understanding of ML277 actions through cell-attached single-channel recordings of wild-type and mutant KCNQ1 channels with voltage sensor domains fixed in resting, intermediate, and activated states. ML277 has profound effects on KCNQ1 single-channel kinetics, eliminating the flickering nature of the openings, converting them to discrete opening bursts, and increasing their amplitudes approximately threefold. KCNQ1 single-channel behavior after ML277 treatment most resembles IO state-locked channels (E160R/R231E) rather than AO state channels (E160R/R237E), suggesting that at least during ML277 treatment, KCNQ1 does not frequently visit the AO state. Introduction of KCNE1 subunits reduces the effectiveness of ML277, but some enhancement of single-channel openings is still observed.

Introduction

The voltage-gated potassium channel, KCNQ1 (Kv7.1), is found throughout the body and, in complexes with accessory subunits, plays important roles in repolarization, ion homeostasis, and hormone secretion (Liin et al., 2015; Liu et al., 2014). In the heart, KCNQ1 assembles with KCNE1 to make up the slowly activating delayed rectifier current (I_{Ks}; Barhanin et al., 1996, Sanguinetti et al., 1996). Loss of function mutations in either of these two subunits can lead to long QT (LQT) syndrome types 1 and 5, respectively, and an elevated risk of sudden cardiac death. To date, pharmacologic treatment of individuals with LQT1 is of an indirect nature and limited to administration of β-adrenergic receptor blockers (Schwartz et al., 2020).

KCNQ1 is structurally a typical voltage-gated potassium (Kv) channel in that it consists of four subunits, each containing six transmembrane domains (TMDs). The first four TMDs make up a peripheral voltage sensor domain (VSD) that is coupled to the pore domain (PD) via a linker between the fourth (S4) and fifth (S5) transmembrane regions. This is referred to as the S4-S5L and is thought responsible for electro-mechanical coupling of VSD movement to pore opening. The biophysical behavior of KCNQ1 is variably altered upon association of any one of five β-subunits, KCNE1-5. In addition, calmodulin is an obligate partner of KCNQ1, where it is required for assembly and trafficking of the channel complex to the cell's surface (Ghosh et al., 2006; Shamgar et al., 2006). PIP2 is also required for channel activity, and binding of the lipid in the region of the S4-S5L (Sun and MacKinnon, 2020) is largely responsible for coupling of VSD activation to pore opening (Loussouarn et al., 2003; Zaydman et al., 2013).

Some effort has been expended to find activators of KCNQ1 and I_{Ks} as a direct therapeutic approach to the treatment of LQT1. Those that have been identified have tended to fall into those that only or mostly activate KCNQ1 ((2R)-*N*-[4-(4-methoxyphenyl)-2-thiazolyl]-1-[(4-methylphenyl)sulfonyl]-2-piperidinecarboxamide; ML277; Yu et al., 2013), zinc pyrithione (Gao et al., 2008), and L-364,373 (Salata et al., 1998); and those that mostly activate I_{Ks} in a 4:4 KCNQ1:KCNE1 stoichiometry, phenylboronic acid (Mruk and Kobertz, 2009), hexachlorophene (Zheng et al., 2012), mefenamic acid (MefA), and 4,4'-diisothiocyano-2,2'-stilbenedisulfonic acid (Busch et al., 1997; Wang et al., 2020). However, after showing little activity on KCNQ1 coexpressed with KCNE1 in expression systems, some of these compounds do shorten the duration of the action potential in isolated myocytes (Xu et al., 2015, Salata et al., 1998). This suggests that the stoichiometry of I_{Ks} in the myocytes, the ratio of KCNQ1 to KCNE1, could be less than a saturating 4:4 or that sequence differences between species are important.

Department of Anesthesiology, Pharmacology and Therapeutics, University of British Columbia, Vancouver, Canada.

Correspondence to David Fedida: david.fedida@ubc.ca.

ML277 is a potent KCNQ1 activator that was developed from a library screen and subsequent refinement process (Mattmann et al., 2012). When exposed to ML277, KCNQ1 peak currents in mammalian cells increase approximately three- to sixfold, activation is shifted ∼15–20 mV more negative, and deactivation slows significantly (Yu et al., 2013, Xu et al., 2015). In addition, elimination of inactivation is thought to contribute to the observed increase in currents (Yu et al., 2013, Hou et al., 2019). Much like several other KCNQ1 activators, the action of ML277 is dependent on the stoichiometry of the KCNQ1/KCNE1 complex, with some finding little (Xu et al., 2015) or no effect (Yu et al., 2013, Hou et al., 2019) of the drug when KCNQ1 is complexed with a saturating level of KCNE1. However, ML277 enhances I_{Ks} in isolated guinea pig and canine ventricular myocytes (Xu et al., 2015) and rabbit atrial myocytes (Kanaporis et al., 2019) in addition to shortening the action potential in these cells, and in human induced pluripotent stem cell (iPSC)–derived cardiomyocytes from healthy controls and LQT1 patients (Ma et al., 2015, Wuriyanghai et al., 2018, Yu et al., 2013). This, as stated earlier and by others (Yu et al., 2013; Xu et al., 2015), suggests that I_{Ks} in myocytes may not be fully saturated with KCNE1, and if this is also true of I_{Ks} in the intact human heart, ML277, or a derivative, could potentially be used as a therapeutic to treat patients with LQT1.

In the current study, we offer new insight into ML277 action on KCNQ1 channels by first being able to examine the drug effects on single channels, and separating effects on voltage gating versus the pore. Our work indicates that increases in single-channel currents in response to ML277 in KCNQ1 and in I_{Ks} complexes with different stoichiometries of KCNQ1 and KCNE1 are at least as important as those induced by changes in deactivation gating. The differential sensitivities of the gating and pore actions of the drug suggest the possibility of multiple binding sites on the KCNQ1 channels, and the particular actions of ML277 in channel constructs that have fixed voltage sensors, stabilized in basal, intermediate, or activated states, illuminate some underlying commonalities between them in the way that they conduct, activate, and inactivate.

Materials and methods

Chemicals

ML277, (*N*-[(3*R*,4*S*)-3,4-dihydro-3-hydroxy-2,2-dimethyl-6-(4,4,4-trifluorobutoxy)-2*H*-1-benzopyran-4-yl]-*N*-methylmetanesulfonamide; HMR1556, referred to as HMR in this article), and *N*-trityl-3-pyridinemethanamine (UCL2077) were obtained from Tocris Biosciences and were dissolved at high concentrations in DMSO and stored at −20°C as per the manufacturer's instructions. They were diluted >1,000-fold in the bathing solutions before the electrophysiological measurements. All other chemicals were obtained from Sigma-Aldrich.

Molecular biology

The tethered constructs of KCNE1 (E) plus KCNQ1 (Q) (EQ, EQQ, EQQQQ, E160R-Q*Q, E160R-QQQ*Q*, E160R-Q*QQ*Q*) were generated as previously described (Murray et al., 2016; Westhoff et al., 2019). The K41C mutation was introduced into EQ using site-directed mutagenesis, confirmed by sequencing, and the mutant KCNE was transferred into EQQ and EQQQQ. The other KCNE1 mutants were generated as described earlier (Wang et al., 2020). R2 (E160R/R231E-Q), R4 (E160R/R237R-Q), and E160R/C314A/G219C/C331A-Q (denoted in figures by Q*) were kind gifts from Jianmin Cui, Washington University, St. Louis, MO. Throughout the paper, the E160R mutation in Q1 is denoted by an asterisk (Q*), and the K41C mutation in E1 is denoted by an apostrophe (E').

Cell culture and transfection

tsA201 transformed human embryonic kidney 293 (TSA; whole-cell experiments) or *ltk*-mouse fibroblast cells (LM; whole-cell and single-channel experiments) were handled as previously described (Murray et al., 2016). There were no observable differences in peak tail current response between the two cell types (data not shown). As a result, the vast majority of whole-cell experiments were conducted in TSA cells because they expressed more current, and LM cells were used for single-channel experiments because they have fewer endogenous channels. Cells plated on coverslips were transfected 24 h later using Lipofectamine 2000 (Thermo Fisher Scientific) as per the manufacturer's protocol. The channel constructs were transfected with GFP in a 3:1 ratio. All experiments were performed 24–48 h after transfection at room temperature. Successfully transfected cells were identified by GFP fluorescence.

Whole-cell and cell-attached patch clamp

Whole-cell currents were acquired using an Axopatch 200B amplifier, Digidata 1440A, and pClamp 10 software (Molecular Devices). A linear multistage electrode puller (Sutter Instrument) was used to pull electrode pipettes from thin-walled borosilicate glass (World Precision Instruments). Pipettes were fire polished before use. Electrode resistances for whole-cell recordings were between 1 and 2 MΩ, with series resistances <4 MΩ. Series resistance compensation of ∼80% was applied to all whole-cell recordings, with a calculated voltage error of ∼1 mV/nA current. Whole-cell currents were sampled at 10 kHz and filtered at 2–5 kHz (Murray et al., 2016; Westhoff et al., 2017).

Single-channel currents were acquired using an Axopatch 200B amplifier, Digidata 1330A, and pClamp 9 software (Molecular Devices). Single-channel electrodes were pulled from thick-walled borosilicate glass (Sutter Instrument) using the linear multistage electrode puller (Sutter Instrument). After fire-polishing, single-channel electrode resistances were between 40 and 60 MΩ. Before use, electrodes were coated with Sylgard (Dow Corning). Current records were sampled at 10 kHz; low-pass–filtered at 2 kHz at acquisition using a −3 dB, four-pole Bessel filter; and digitally filtered at 200 Hz for presentation and analysis (Werry et al., 2013; Eldstrom et al., 2015; Murray et al., 2016; Thompson et al., 2017; Westhoff et al., 2017).

Electrophysiology solutions

For whole-cell recordings, the bath solution contained (in mM) 135 NaCl, 5 KCl, 1 $MgCl_2$, 2.8 NaAcetate, and 10 HEPES (pH 7.4, with NaOH). The pipette solution contained (in mM) 130 KCl, 5 EGTA, 1 $MgCl_2$, 4 Na_2-ATP, 0.1 GTP, and 10 HEPES, pH 7.2, with

KOH. For single-channel recordings, the bath solution contained (in mM) 135 KCl, 1 $MgCl_2$, 1 $CaCl_2$, 10 HEPES, and 10 dextrose, pH 7.4, with KOH. The pipette solution contained (in mM) 6 NaCl, 129 Mes, 1 $MgCl_2$, 5 KCl, 1 $CaCl_2$, and 10 HEPES, pH 7.4, with NaOH.

Analysis

G-V plots were obtained from normalized tail current amplitudes. A Boltzmann sigmoidal equation was used to fit G-Vs (Prism 9; GraphPad Software) to obtain the half-activation voltage ($V_{1/2}$) and slope factor. Gaussian fits of all-points histograms of single-channel events (using 0.01-pA bin widths) were obtained in Clampfit 10 (Molecular Devices).

Concentration-response curves were generated by normalizing the ML277 peak tail current values from +60 test pulses to the peak control amplitude for data collected from the same cell. Normalized values were then plotted against ML277 concentration and fit with an [Agonist] versus response (three parameters) function in Prism to obtain half maximal effective concentrations (EC_{50}s).

All results are reported as mean ± SEM, unless otherwise stated. Statistical comparison was performed in Prism using one-way ANOVA, two-tailed Student's *t* test, or Mann–Whitney test. P values <0.05 were considered to be statistically significant.

Online supplemental material

Fig. S1 includes KCNQ1 diary plots after ML277 and HMR addition, concentration-response curves for HMR, and peak tail current changes at different voltages. Fig. S2 contains additional G-V data for EQQQQ, EQQ, EQ, Q*Q, QQQ*Q*, Q*QQ*Q*, and Q*QQQ as well as a plot of deactivation time constants versus voltage for EQ, EQQ, and EQQQQ. Fig. S3 shows the tail currents after HMR block of Q* channels and a GFP transfected cell treated with ML277, as well as data from the S338F mutant of KCNQ1.

Results

ML277 increases the amplitude of KCNQ1 whole-cell and single-channel currents

As previously described, there is a dramatic increase in peak current, a slowing of deactivation, and a loss of voltage-dependent gating upon exposure of KCNQ1 to 1 µM ML277 (Fig. 1; Yu et al., 2013, Xu et al., 2015). The change in peak current has a relatively fast onset, within ∼30 s of bath application, as shown in Fig. 1 A. In this example, the entire bath contents were replaced with ML277-containing solution during trace 4, and no change is observed in trace 5, but a dramatic increase in peak current is evident during trace 6 (pulses applied every 15 s), which stabilizes by trace 8. The magnitude of the response was variable as shown in Fig. S1, A, C, and D. The enhanced current is sensitive to HMR with a half-maximal inhibitory concentration (IC_{50}) of around 3.5 µM, though this increases to nearly 6 µM if the ML277 is not washed out of the bath (Fig. S1, B and E). 0.1% DMSO alone was also tested on KCNQ1, and while there was no effect on the $V_{1/2}$ of activation, a nonsignificant decrease in tail currents was observed (mean decrease of 14.0 ± 6.2%; n = 5; Fig. S1 F).

Voltage-dependent gating of KCNQ1 appears to be greatly reduced upon exposure to ML277 using a protocol with a 15-s interpulse interval (Fig. 1 B). During these longer 4-s pulses, although activation appears almost constitutive, inactivation of KCNQ1 is seen to be preserved in the presence of ML277 at higher pulse potentials. However, during test pulses to +60 mV using longer interpulse intervals of 30 or 60 s, the channels do appear able to fully deactivate as the instantaneous current at the start of the test pulses returns to control levels (Fig. 1 A, bottom). The effect of ML277 on peak tail currents was measured without contamination from endogenous currents in both TSA and LM cells (which deactivate much faster at −40 or −50 mV). ML277 increased KCNQ1 tail currents by 8.5 ± 1.8-fold at +60 mV at a concentration of 1 µM (Fig. 1 D; and Fig. S1, C and D). The complete voltage-dependence of the concentration-response to ML277 is shown in Fig. 1 C and illustrates the complexity of the drug action on this channel. These data are normalized to the largest tail current in each case, which occurs at positive potentials in control due to channel activation gating and at progressively more negative voltages at higher doses of ML277 due to constitutive activation in ML277, and the persistence of inactivation. At the lowest dose of 100 nM, ML277 shifted the G-V curve −11.8 mV and increased current size, but higher concentrations flattened the curves and resulted in the 1-µM and 2-µM ML277 G-V curves converging at the highest voltages. The EC_{50}, measured from tail currents at +60 mV from data normalized to the control value at +60 resulted in a value of 100 nM (Fig. 1 D).

One way to determine if ML277 is simply modifying gating or has other effects on the channel is to carry out single-channel recordings. Usually, single-channel recordings enable measurement of open probability and channel conductance, either of which could lead to an increase in current observed at a whole-cell level. As we have published previously, though (Hou et al., 2017), KCNQ1 single-channel openings are very small-amplitude (∼0.02 pA; Fig. 1 E), hard to separate from the noise, and often very brief, giving a flickery appearance. This makes them very difficult to record and to accurately describe quantitatively given the frequency limitations of the recording system. However, exposure to 1 µM ML277 increased the apparent amplitude of openings (0.069 ± 0.003 pA; Fig. 1 E) and prolonged burst durations of KCNQ1 under our recording conditions, making events much more obvious and easier to measure as shown by the all-points histogram, where opening events are now distinguishable as a separate peak from closings (Fig. 1 G). Ensemble averages of 17 active traces of KCNQ1 and KCNQ1 + ML277 show the increase in current size overall as well as the obvious increase in the tail current amplitude on drug exposure (Fig. 1 F). From these data, it is clear that open event durations have increased, but in WT KCNQ1, it is not possible to discriminate between a change in VSD activation or increased VSD–pore coupling that stabilizes the open state. Similarly, it cannot be determined whether the increased opening amplitudes are secondary to the longer open times or represent an increased maximum channel conductance. That these changes can be attributed to KCNQ1 channels, though, can be demonstrated by the ML277-enhanced single-channel current sensitivity to HMR (Fig. S1 G).

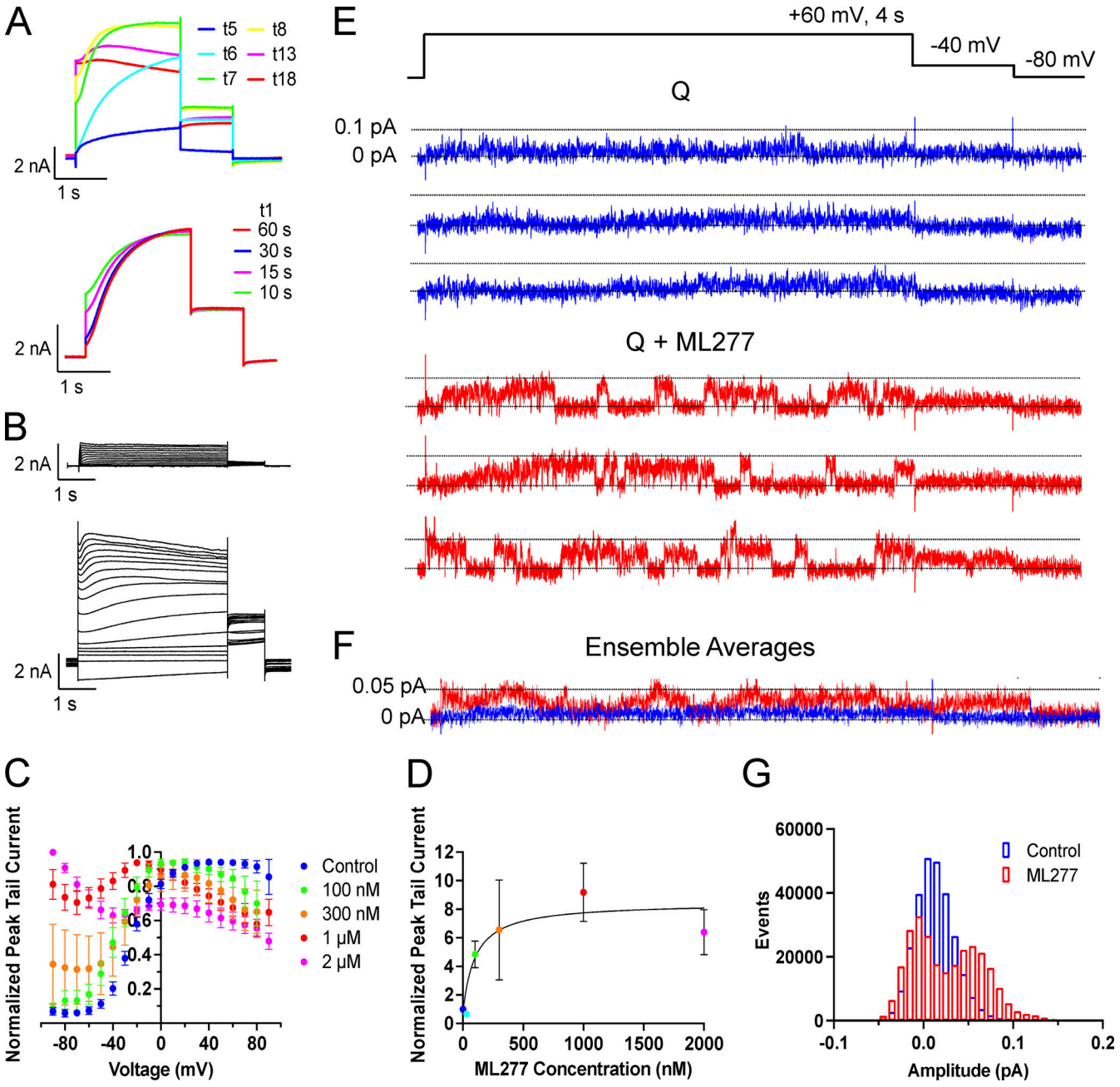

Figure 1. **KCNQ1 responds to ML277 with a large increase in current. (A)** Top: Representative KCNQ1 current traces (t) just as (t5) and after 1 µM ML277 was added to the bath. Cell was pulsed from a holding potential of −80 mV to +60 mV for 2 s, then for 1 s to −40 mV. The interpulse interval was 15 s. Bottom: Effect of increasing interpulse intervals at a holding potential of −80 mV on current waveform at +60 mV for 2 s in the presence of 1 µM ML277. Trace t1 obtained in control solution, others after rest intervals as indicated in the presence of ML277. **(B)** Representative KCNQ1 currents in control (top) and in 1 µM ML277 conditions (bottom), obtained using 4 s voltage-clamp pulses from −90 to +80 mV in 10 mV steps. Interpulse interval was 15 s, and tail currents were measured at −50 mV for 1 s. **(C)** Normalized G-V plots for KCNQ1 obtained from peak tail currents at different concentrations of ML277 as indicated (n = 5–11). The $V_{1/2}$ for KCNQ1 in control conditions was −20.9 ± 2.3 mV. **(D)** ML277 concentration-response curves at +60 mV using tail current data normalized to same cell control values and fit with drug versus response, three parameter curves to obtain EC_{50}s using GraphPad software, n = 2–6. **(E)** Representative single-channel recordings of GFP-tagged KCNQ1 in control conditions above (blue) and in 1 µM ML277 below (red) from the same patch. The voltage protocol is shown above the control sweeps, and the interpulse interval was 10 s. **(F)** Ensemble averages of 17 active sweeps of control KCNQ1 (blue trace) and after 1 µM ML277 treatment (red trace). Control traces were combined from two different patches including patch shown in A and B. ML277 traces were only from the patch shown. **(G)** All-points histograms of 40 KCNQ1 single-channel sweeps in control (blue bars) and 40 sweeps in 1 µM ML277 (red bars).

KCNE1 and ML277

Previous studies have shown that when high levels of KCNE1 are expressed with KCNQ1, the complex becomes insensitive to ML277, and that a 2:4 stoichiometry of E1:Q1 shows only a modest increase in currents (Yu et al., 2013). We found that even the addition of one KCNE1 reduced the ability of ML277 to enhance current amplitudes (Fig. 2, A and B) such that there was no difference in the tail current increase induced by ML277

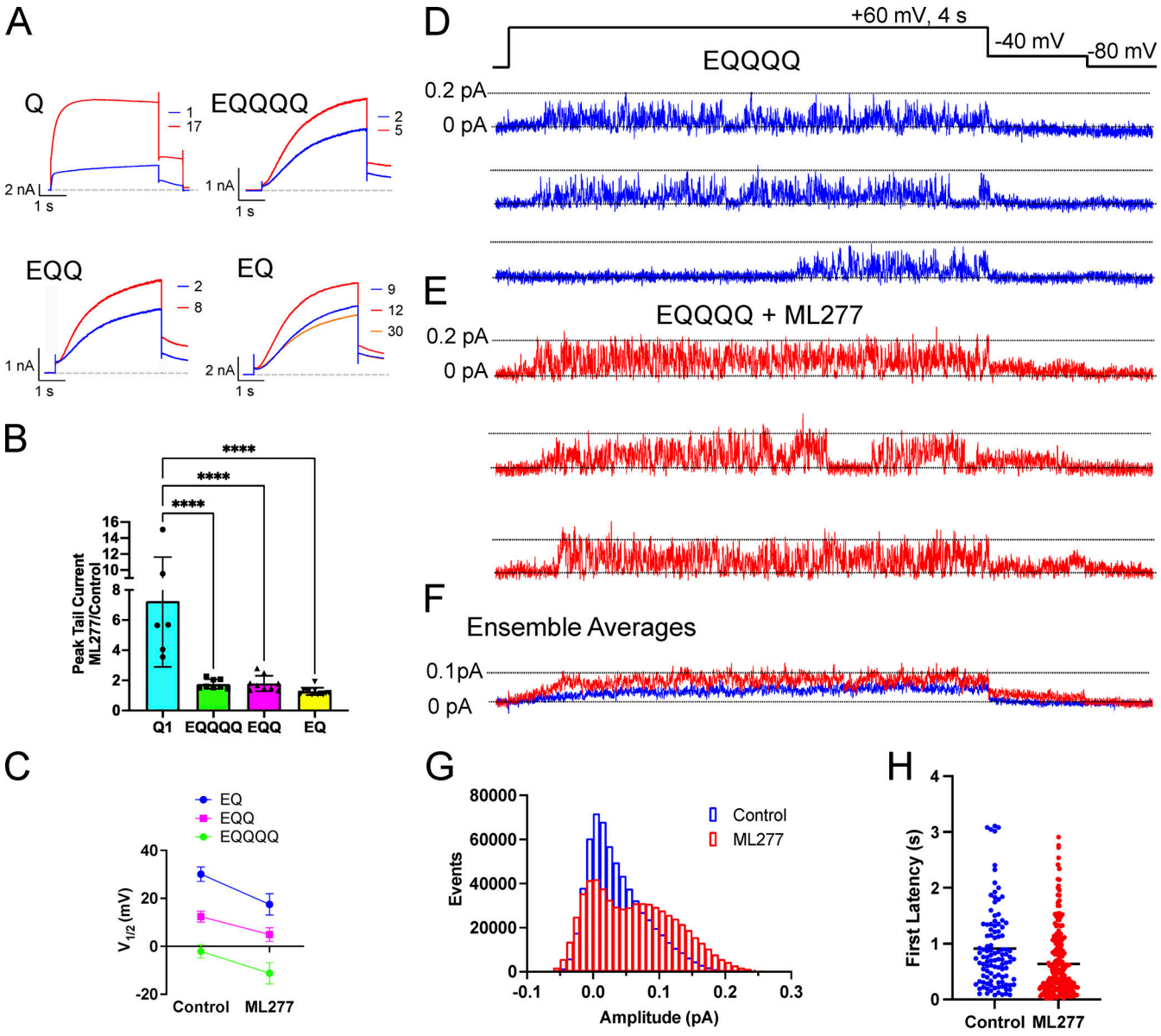

Figure 2. **ML277 increases amplitude of EQQQQ openings. (A)** Representative whole-cell current traces from cells before (blue trace) and after exposure to 1 µM ML277 (red trace) for channel complexes containing increasing numbers of KCNE1. The example for EQ shows an extra sweep in orange to highlight the current rundown that took place after 8 min recording. **(B)** Bar chart showing the tail current amplitude in ML277 divided by control amplitude for Q1 and WT I_{Ks} of different stoichiometries. ****, P < 0.0001. **(C)** $V_{1/2}$ of activation before and after 1 µM ML277 treatment for EQ, EQQ, and EQQQQ (n = 6–12). See Table 1 for slope factors. All error bars denote mean ± SEM. **(D and E)** Representative single-channel recordings of EQQQQ in control (D) and in 1 µM ML277 (E) from the same patch. The voltage protocol is shown above the control sweeps, and the interpulse interval was 10 s. **(F)** Ensemble average currents of 16 active sweeps in control EQQQQ (blue trace) and after 1 µM ML277 treatment (red trace) from the same patch. **(G)** All-points histograms of the same data used in F. **(H)** First latencies for EQQQQ in control and ML277 conditions. Mean first latencies were 0.91 ± 0.07 s for control (108/287 active, 38%) and 0.64 ± 0.04 s in the presence of ML277 (223/703 active, 32%), n = 3.

between EQ (4:4), EQQ (2:4), and EQQQQ (1:4). A 2-µM dose was tried on EQQ (not shown), but this produced only a minor increase from the 1-µM ML277 dose. Overall, a 10-mV hyperpolarizing shift in the voltage-dependence of activation was observed for EQQQQ with ML277 treatment (Fig. S2 and Table 1) as measured from the G-V relationships obtained from peak tail currents. The $V_{1/2}$s of activation across all KCNE1-containing constructs in the presence of ML277 were significantly different from their control values (Fig. 2 C and Fig. S2). However, the impact on deactivation was much greater, with EQ (4:4) showing no change in the rate of deactivation on ML277 treatment and EQQQQ showing the most slowing at voltages between −50 and −70 mV (Table 2 and Fig. S2 H). The EQ construct was more likely than the other constructs to show a decrease in current after a brief increase, as shown by the orange sweep in Fig. 2 A (bottom right), which was recorded 3 min after the ML277 effect peaked.

At the single-channel level, 1 µM ML277 is also able to increase the amplitude of openings through EQQQQ channels, but

Table 1. **$V_{1/2}$ of activation and slope of G-V plots**

		Control			ML277		P value
Construct	**$V_{1/2}$ (mV)**	**Slope**	***n***	**$V_{1/2}$ (mV)**	**Slope**	***n***	
EQ	30.1 ± 3.0	21.9 ± 1.0	12	17.5 ± 4.5	21.2 ± 1.5	10	0.003
EQQ	12.4 ± 2.3	19.0 ± 1.3	9	4.9 ± 2.9	18.5 ± 0.9	7	0.006
EQQQQ	−1.3 ± 2.2	18.0 ± 2.5	8	−12.3 ± 3.8	16.5 ± 2.0	6	0.031
Q	−20.9 ± 2.3	10.5 ± 2.0	4				-
Q*QQQ	−10.3 ± 4.8	18.6 ± 2.1	4				-
Q*Q	3.5 ± 2.2	15.6 ± 1.3	7	−0.5 ± 7.5	14.6 ± 3.8	3	ns
QQQ*Q*	−13.3 ± 2.8	17.2 ± 2.1	4	−14.2 ± 1.5	13.5 ± 1.2	3	ns
Q*QQ*Q*	5.4 ± 4.6	13.5 ± 1.5	6	7.6 ± 3.0	15.9 ± 1.0	4	ns
K41C-E'QQQQ	−9.0 ± 7.4	16.3 ± 3.1	3				-
K41C-E'QQ	−7.0 ± 2.3	20.1 ± 1.7	6	−50.9 ± 10.9	45.8 ± 5.39	5	0.0003
KCNE5-Q	~134	~35	3	~54	~60	4	

$V_{1/2}$ of activation was obtained from −40 mV tail portion of voltage-clamp protocols (−90 mV holding potential, pulsed from −90 up to +60 to +100 mV in 10 mV steps for 4 s, then to −40 mV for 1 s). Statistical comparison was performed using unpaired *t* tests in GraphPad Prism.

the openings remain flickery. The increase is easier to see in EQQQQ channels, which have a larger conductance than KCNQ1 channels, and the action of ML277 is clear from both the individual traces (Fig. 2, D and E) and the ensemble averages (Fig. 2 F), where deactivation is slowed. The all-points histograms of equal numbers of active sweeps show that higher openings are achieved with a clear second peak evident at ~0.08 pA, which is not the case in control data (Fig. 2 G). There is also a decrease in the number of closed events, which is in part a result of a decrease in the latency to first opening (Fig. 2 H). The mean first latency for EQQQQ in control conditions was 0.91 ± 0.07 s (108/287 active, 38%) and 0.64 ± 0.04 s in the presence of ML277 (223/703 active, 32%). ML277 showed similar effects on EQQ and EQ single channels (Fig. 3 A), with more frequent and larger amplitude events as shown in the all-points histograms (Fig. 3 B), which were at least in part due to significantly shortened first latencies (Fig. 3 C and Table 3). 39% of control EQQ traces were active (138/356) versus 58% of ML277 traces (347/602). In control conditions, 21% of EQ traces were active (123/597), and 14% were active in ML277 (116/835).

Constitutively activated KCNQ1 channels respond to ML277

Fixed, activated KCNQ1 mutants involve charge reversal mutations between the S2 and the S4 in the VSD that effectively "lock" the VSD (Fig. 4, A and B) in an intermediate-activated state (E160R/R231E, in this paper referred to as R2) or a fully activated state (E160R/R237E, referred to as R4; Zaydman et al. 2014). Since these mutants have a fixed activation, any increase in current observed would be the result of enhanced VSD–pore coupling, increased conductance, or change in inactivation. Both of these VSD mutants respond quite robustly to 1 μM ML277 (Fig. 4, A and B), with R2 tail currents increasing ~3.5 fold (3.75 ± 0.59) and R4 increasing ~6-fold (5.86 ± 1.30; Fig. 4 C), but as the complete voltage-dependence of their concentration-responses to ML277 shows in Fig. 4 D for R2 and R4, there is an important difference between them. For R2, the activation gating effects of the drug are removed, and there is a monotonic decline of the concentration-response relationships with potential, reminiscent of the effect of inactivation in Q1 alone (Fig. 1 C). For R4, while the effect of ML277 on activation gating is removed, there is no residual effect of inactivation. It should be noted that the control currents for R4 were very small, and when normalized, there is an exaggerated effect of the small increase in current at the more positive voltages. The EC_{50}s from data collected at +60 mV and normalized to the peak tail current collected before drug addition were 41.4 and 66.2 nM for R2 and R4, respectively (Fig. 4 E). From these two sets of data (Fig. 4, D and E), it seems, were it not for inactivation, R2 would have responded equally as well to ML277 as R4.

Single-channel recordings of R2 show a similar response to ML277 treatment as KCNQ1 (Fig. 5, A and B), with small flickering openings transitioning to larger, more stable openings. Averaged Gaussian fits of the all-points histograms identified two peaks of 0 and 0.02 pA in control conditions and 0 and 0.073 pA in ML277 (Fig. 5, C and E). Interestingly, R4 while responding alike in terms of having larger, more stable openings than in control conditions (Fig. 5 D), had smaller openings than R2, with the nonzero peaks of the amplitude histograms averaging 0.021 ± 0.003 pA for control and 0.050 ± 0.0037 pA in ML277 (Fig. 5, C and E).

KCNQ1 channels with closed state restrained VSD still respond to ML277

To explore the importance of the VSD positioning in the ML277 effects, we also studied channels with increasing numbers of subunits containing the E160R mutation alone, which prevents VSD activation (Fig. 6 A; Westhoff et al., 2019). This would tell us if the VSD needed to approach the PD or the S4-S5L needed to move to create the binding site for ML277 and have an effect. All of the E160R mutants we tried responded to ML277 with an

Table 2. **Deactivation rates for EQ, EQQ, and EQQQQ before and after ML277 treatment**

	Mean (s)	SEM	*n*	Mean (s)	SEM	*n*	P value
Voltage (mV)	**EQ**			**EQ + ML277**			
–50	1.65	0.09	10	1.53	0.06	7	ns
–60	1.82	0.12	9	1.60	0.05	7	ns
–70	1.53	0.36	8	1.81	0.10	5	ns
–80	0.76	0.03	10	0.60	0.04	8	ns
–90	0.70	0.03	10	0.60	0.04	8	ns
–100	0.57	0.03	10	0.50	0.02	8	ns
	EQQ			**EQQ + ML277**			
–50	1.39	0.20	7	2.55	0.16	5	P = 0.0004
–60	1.08	0.14	7	2.42	0.15	5	P < 0.0001
–70	0.74	0.10	6	2.62	0.52	5	P < 0.0001
–80	0.54	0.10	5	1.30	0.12	4	ns
–90	0.43	0.07	6	1.08	0.10	5	ns
–100	0.47	0.06	3	0.98	0.16	3	ns
	EQQQQ			**EQQQQ + ML277**			
–50	1.02	0.14	5	2.18	0.26	4	P = 0.0008
–60	0.78	0.15	5	2.52	0.53	3	P < 0.0001
–70	0.69	0.08	5	2.26	0.29	5	P < 0.0001
–80	0.40	0.10	5	1.35	0.23	5	P = 0.0071
–90	0.38	0.11	6	1.35	0.22	5	P = 0.0016
–100	0.26	0.01	3	0.90	0.08	3	ns

To obtain tail currents for measurement of deactivation rates, cells were held at –80 mV, and pulsed to +60 mV for 4 s followed by a 10-s pulse to a range of potentials from –50 to –100 mV in 10-mV steps. Exponential fits and one-way ANOVA statistical comparison were performed using GraphPad Prism.

increase in current, whether there were one, two, three, or four E160R-containing subunits in the channel complex (Fig. 6 A). Channels with more movable subunits showed larger increases than those with fewer or even none (Fig. 6 B). We noted that KCNQ1 currents can increase without any moving VSD, with an average fold increase of 2.49 ± 0.26 (Fig. 6, A and B). To rule out an endogenous current being responsible for this increase, GFP-only transfected cells were exposed to ML277, and in the absence of KCNQ1, endogenous currents decreased upon ML277 treatment (Fig. 6, A and B). In addition, this current through channels with four E160R-containing subunits was sensitive to HMR and returned on washoff of the blocker (Fig. S3 A). This supports the notion that the currents being recorded from E160R-Q*-transfected cells (four resting VSD) are through "uncoupled" channels, i.e., channels that open independent of the VSD status (Ma et al., 2011). Data in Fig. 6 C show the median and range of peak tail currents for each construct before and after ML277 treatment.

Looking at the two constructs containing E160R in either adjacent subunits (QQQ*Q*; at least one subunit with a moving VSD next to another moving VSD) or opposite subunits (Q*Q; no moving subunit with a moving VSD next door), there was no difference in the magnitude of current increase on ML277 treatment, so these data are combined in Fig. 6 B, but with the Q*Q data points colored green. In one of three cells of the Q*Q configuration exposed to 1 µM ML277, there was a significant fraction of voltage-independent current (shown in Fig. S2 B), which was subsequently seen in four of four cells when the dose of ML277 was increased to 2 or 3 µM (Fig. 6 D). The QQQ*Q* and Q*QQ*Q* constructs also responded to higher doses with an increase in the fraction of voltage-independent current (Fig. S2). This suggests that gating effects are at the level of individual subunits as long as the dose is high enough to find the moving VSD in the complex. This is reflected in a higher EC_{50} value of 235 nM from the concentration-response curve (Fig. 6 E) compared with WT Q1 (100 nM; Fig. 1 D).

ML277 and voltage-dependent state occupancy

In whole-cell recordings of KCNQ1 plus ML277, currents showed a slight decline over time at higher voltages during the 4-s test pulse (Fig. 1 B). In the tail currents of these recordings, the more negative voltages had larger amplitudes than the more positive voltages, as shown in Fig. 7 A, where only the –20 and +60 mV traces are shown. We took advantage of an approximately three-channel KCNQ1 cell-attached patch that lasted long enough in ML277 to collect multiple traces at –20, 0, +20, and +60 mV, to look at this more closely. As can be seen in Fig. 7 B, it was rare for all three channels to be open at +60 mV (upper trace) and rare

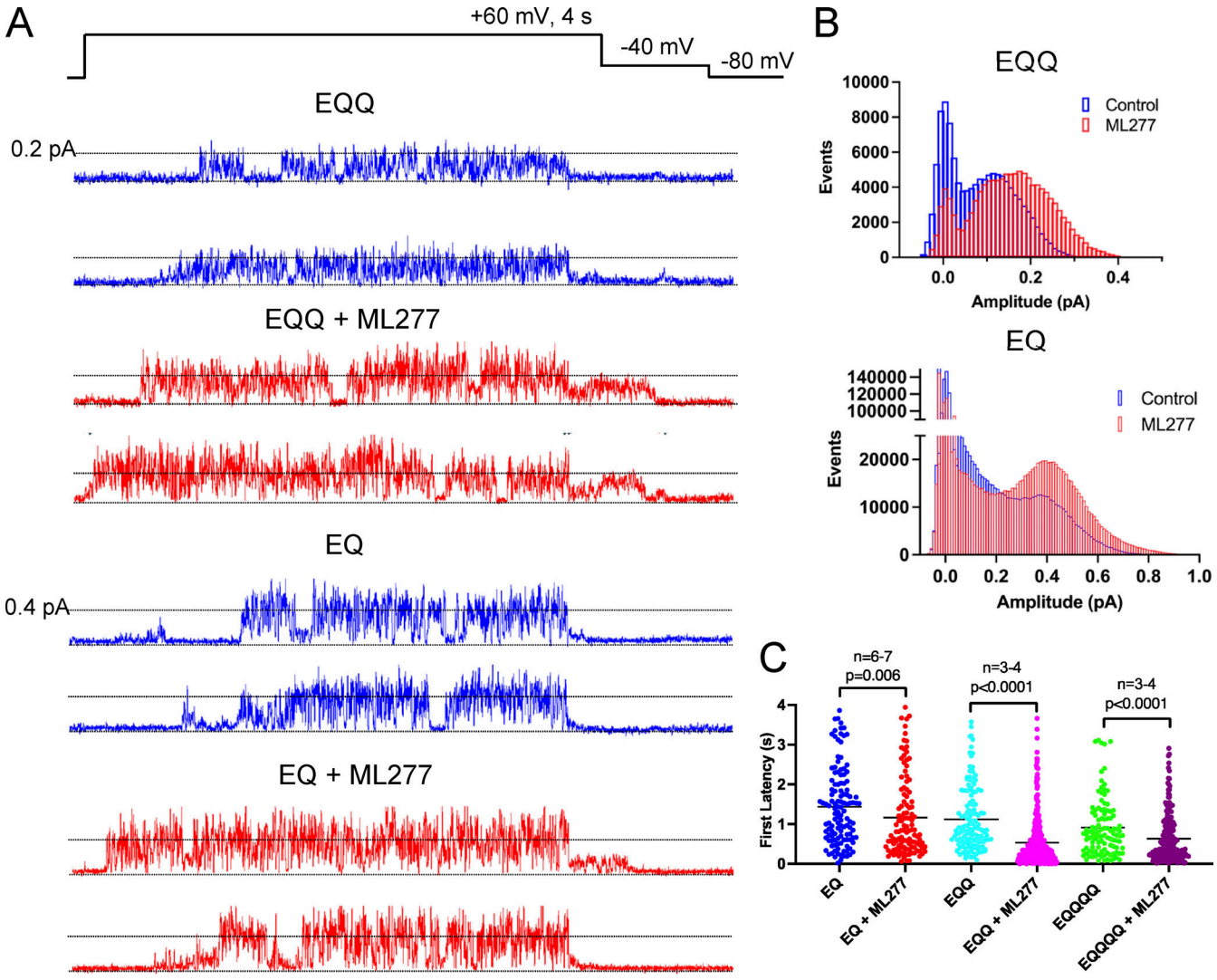

Figure 3. **ML277 increases the amplitude of EQQ and EQ openings. (A)** Single-channel recordings of EQQ (top) and EQ (bottom) before (blue traces) and after addition of 1 µM ML277 (red traces) from the same patch as control data. The voltage protocol is shown above the data. **(B)** All-points amplitude histograms of three active sweeps of EQQ before (blue) and after 1 µM ML277 addition (red; top) and 27 active sweeps combined from three different cells of EQ before (blue) and after 1 µM ML277 addition (bottom). **(C)** Scatter plot of first latencies to opening of the active sweeps for EQ, EQQ, and EQQQQ before and after ML277 exposure. See Table 3 for mean values.

for all three channels to be closed at −20 mV (lower trace). The percent closed time for all sweeps collected at each voltage was measured using the single-channel search function based on a half-amplitude criterion. During 10 traces pulsed to −20 mV, each of 4 s duration, the percent time closed was 0.3%. At 0 (20 traces), +20 (10 traces), and +60 mV (55 traces), the percent closed times were 0.6, 2.6, and 29.8%, respectively. As was observed in the whole-cell recording (Fig. 7 A), the amplitudes of

Table 3. **First latency to channel opening for EQ, EQQ, and EQQQQ before and after ML277 treatment**

	Control			ML277			
	Mean ± SEM	**No. of cells**	**Active/total**	**Mean ± SEM**	**No. of cells**	**Active/total**	**P value**
EQ	1.44 ± 0.09	7	123/587	1.16 ± 0.09	6	116/835	P = 0.006
EQQ	1.12 ± 0.07	5	138/356	0.54 ± 0.03	4	347/602	P < 0.0001
EQQQQ	0.91 ± 0.07	3	108/287	0.64 ± 0.04	3	223/703	P < 0.0001

First latencies were obtained from 4-s sweeps pulsed to +60 mV. Only active sweeps were used for averages. Statistical comparison was performed using a Mann–Whitney test in GraphPad Prism.

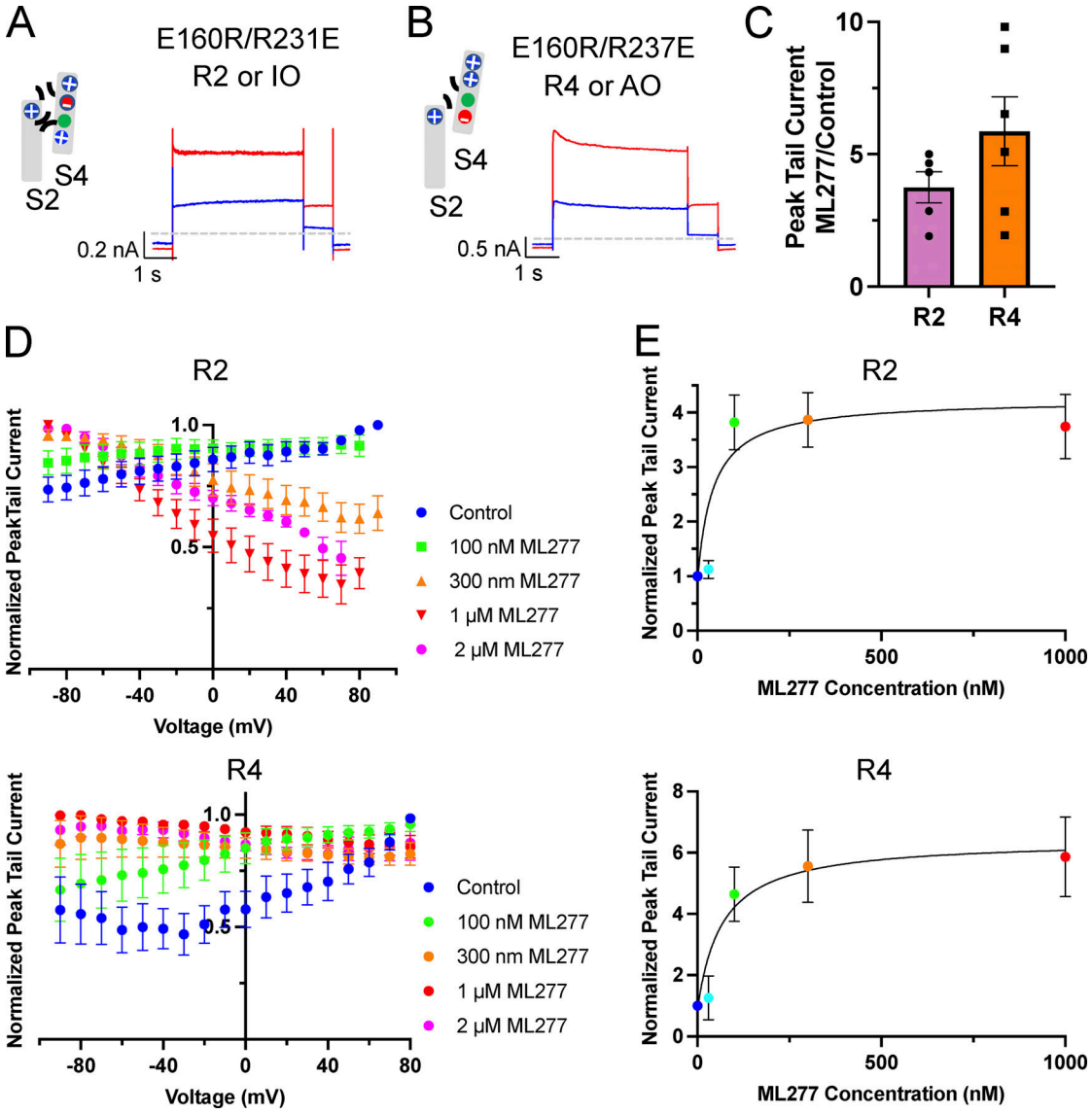

Figure 4. **R2 and R4 mutants also respond to ML277 with an increase in current amplitude. (A and B)** Cartoons representing the putative interactions between the charges in the S2 and S4 TMDs of the VSDs that hold them in the IO state (R2; A) and the AO state (R4; B). Next to the cartoons are representative whole-cell current traces from cells before (blue trace) and after exposure to 1 µM ML277 (red trace). Cells were held at −90 mV and pulsed for 4 s to +60 mV and then −40 mV for 0.8 s. Interpulse interval was 15 s. **(C)** Bar chart of peak tail currents measured in ML277 divided by control peak current measurement for R2 (n = 4) and R4 (n = 5). The mean ratio ± SEM for R2 is 3.75 ± 0.59, and for R4 it is 5.86 ± 1.30. **(D)** Normalized G-V plots for R2 (top) and R4 (bottom) obtained from peak tail currents at different concentrations of ML277 as indicated (n = 3–11). Voltage protocol was the same as for A and B. **(E)** ML277 concentration-response curves at +60 mV for R2 (n = 3–8) and R4 (n = 2–6), using tail current data normalized to same cell control values and fit with drug versus response. Three parameter curves were used to obtain EC_{50}s using GraphPad software.

the tail currents in ensemble averages are larger from the −20 mV pulse than from the +60 mV (data not shown). After pulsing to −20 mV, most of the channels are open during the tail (Fig. 7 C), whereas after pulsing to +60 mV, openings are more evenly distributed between one and two channels being open. The amplitude of KCNQ1 + ML277 single-channel openings at −40 mV is 0.03 pA.

Although R2 and R4 do not show time-dependent activation due to their VSDs being locked in activated states, we measured tail currents after pulses to different voltages for these constructs also. In the presence of 2 µM ML277, like KCNQ1, R2 tails decline as the voltage becomes more positive and show larger amplitude tail currents at −20 compared with +60 mV (Fig. 7 D). An approximately two-channel cell-attached patch of R2 in 1 µM ML277 was pulsed for 4 s to voltages from −80 to +110 mV in 10-mV steps, and shown in Fig. 7 E are the +60 and −20 traces. This channel too shows rare openings of both channels at +60 mV (upper trace) and rare closings of both channels at −20 mV (lower trace).

We had one recording each of single-channel patches of R2 and KCNQ1 in which we were able to run voltage-clamp protocols similar to those used for whole-cell recordings after treatment with ML277. Cells were held at −80 mV and pulsed to voltages between −80 and +110 mV in 10-mV steps for 4 s each. Using the single-channel search function in Clampfit, closed times

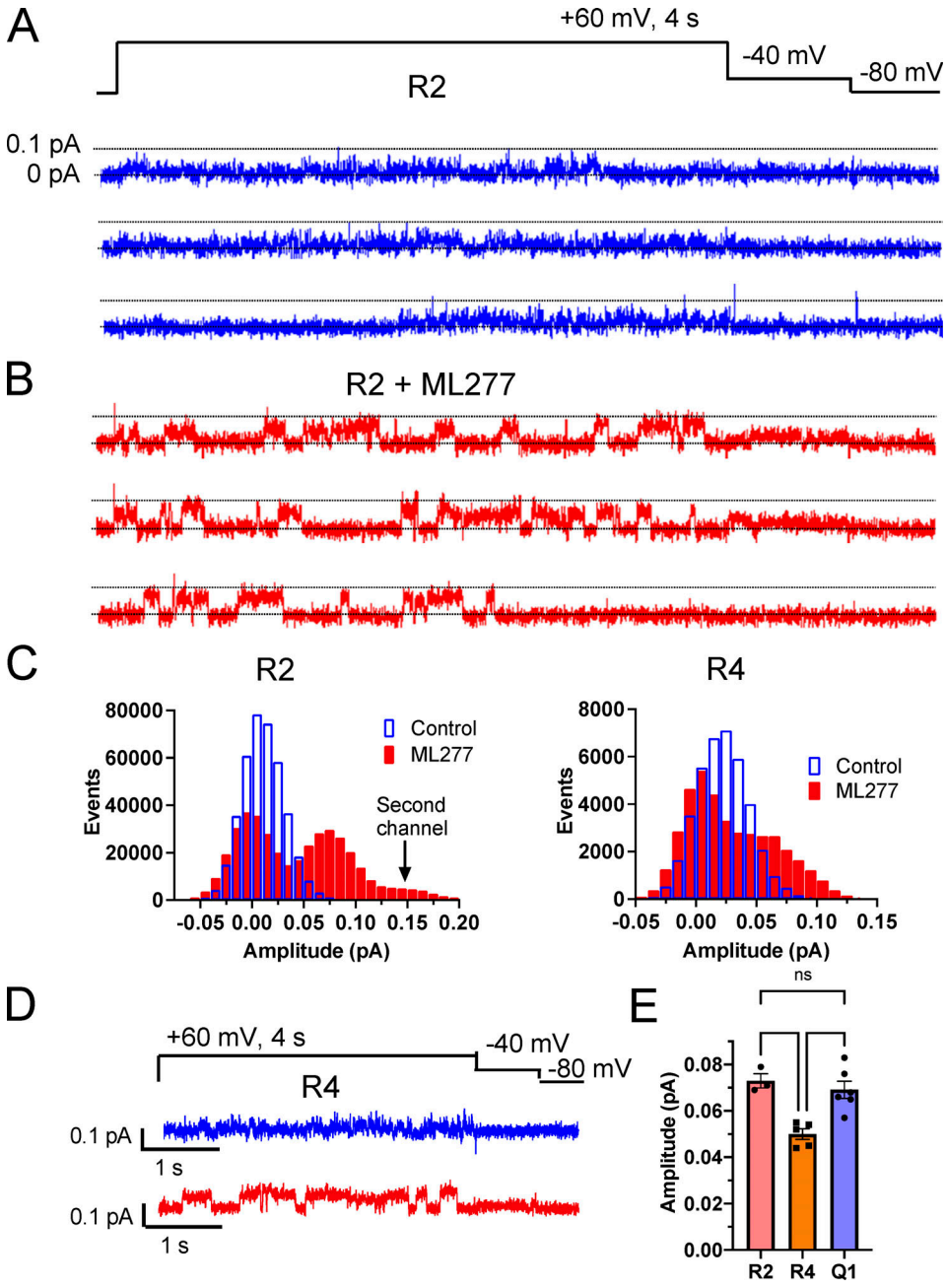

Figure 5. **Increased single-channel current amplitudes in R2 and R4 mutants with ML277. (A and B)** Representative single-channel recordings of R2 in control (A) and in 1 µM ML277 (B) from the same patch. The voltage protocol is shown above the control sweeps, and the interpulse interval was 10 s. **(C)** All-points histograms of 10 R2 single-channel recording sweeps in control (blue) and 10 sweeps in 1 µM ML277 (red) from the same patch. All-points histograms of R4 single-channel sweeps (right). **(D)** Representative sweeps of single-channel recordings of R4 in control conditions (upper sweep) and in 1 µM ML277 (lower sweep) from the same patch. The voltage protocol is shown above the control sweeps, and the interpulse interval was 10 s. **(E)** Amplitudes of openings for R2, R4, and KCNQ1 after exposure to ML277 as determined by Gaussian fits of all-points histograms. Error bars denote mean ± SEM.

were then measured at each voltage (Fig. 7 F). Some of the lower voltages were not measured as it was difficult to discern the closed state, but what is evident from this analysis is that the open probability is decreasing with increasing voltage in both the whole-cell and multi-channel patch data. R2 and KCNQ1 appear to respond in a similar manner to increasing voltage in the presence of ML277.

These single-channel results are supported by the whole-cell voltage dependence of tail current amplitudes for R2, which shows that tail currents are >50% smaller at +80 than they are at −80 mV in the presence of 2 µM ML277 (Fig. 7 G). This is very similar to the trend for the voltage-dependent action of ML277 on Q1 tail currents (Fig. 1 C) but, interestingly, not for R4, which does not show this decline (Fig. 7 G). Despite the differences in G-V curves, there was no statistical difference in the change in KCNQ1 tail current amplitudes between the different doses of ML277 (Fig. 7 H).

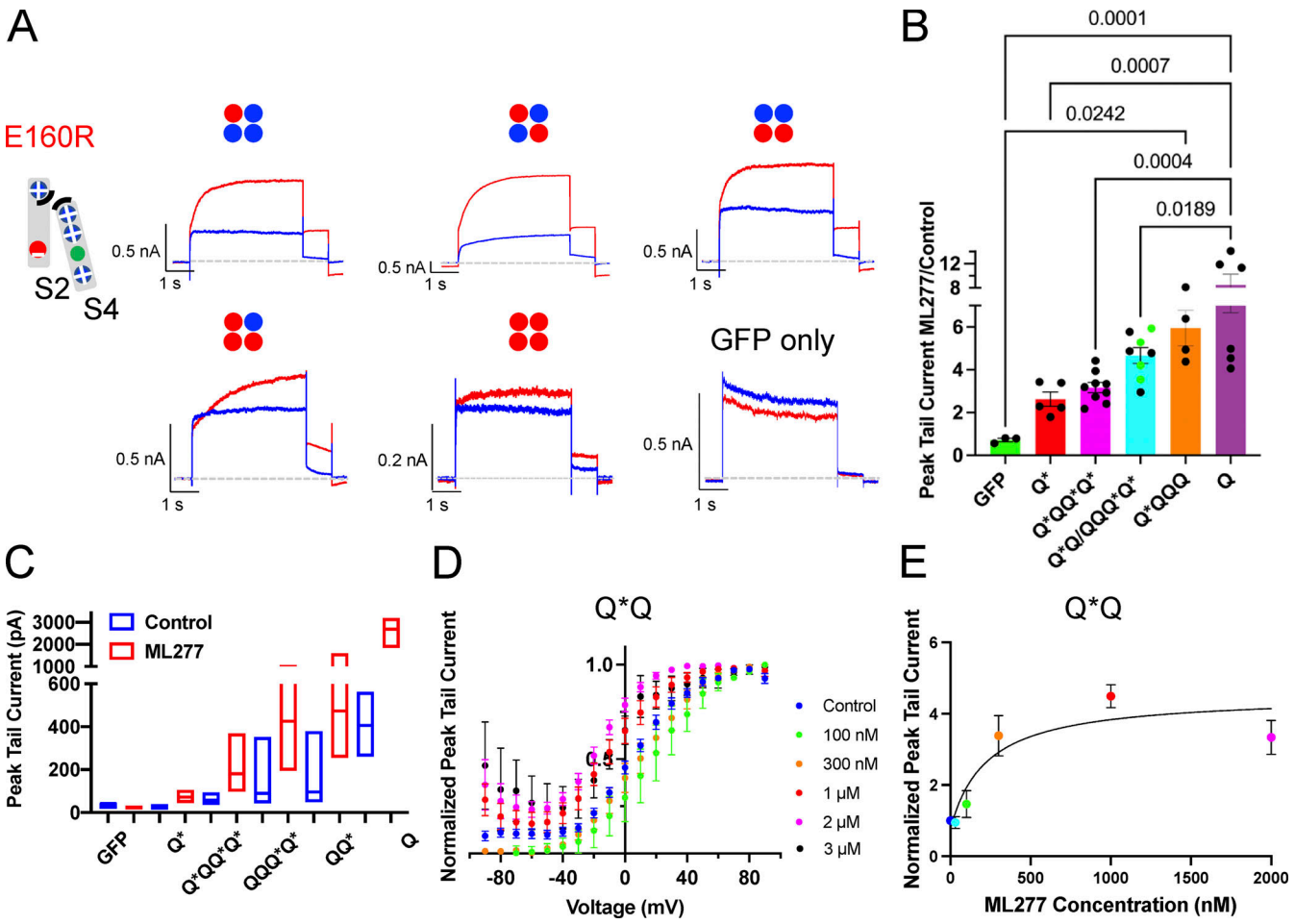

Figure 6. **KCNQ1 mutants with 1–4 VSD restrained in the closed state respond to ML277 with an increase in current. (A)** Cartoon shows the putative interactions between charges in S2 and S4 in the E160R mutant. Cartoons above each representative whole-cell recording denote the number and location of subunits in the channel tetramer containing WT (blue circle) or E160R subunits (red circle). Protocol is as in Fig. 4, A and B. Control traces are blue, and those in 1 µM ML277 are red. A sample from a GFP-only transfected cell is also shown. **(B)** Graph of the ratio of peak tail currents in ML277 to control for different channel complexes. Subunits containing E160R are denoted by an *. **(C)** Bar chart showing the median and range of tail current amplitudes for each channel type before (blue bars) and after ML277 (red bars). **(D)** G-V plots of Q*Q from peak tail currents at −40 mV, shown in control (blue circles), and at different concentrations of ML277 as indicated. All error bars denote mean ± SEM (n = 3–15). **(E)** ML277 concentration-response curves at +60 mV using tail current data normalized to same cell control values and fit with drug versus response. Three parameter curves to obtain EC_{50}s using GraphPad software, n = 3–7.

Discussion

An important finding of this study is that in addition to changing the whole-cell gating, ML277 substantially changes KCNQ1 single-channel behavior in a number of ways. The activator eliminates the characteristic KCNQ1 flicker, making the openings much more stable and larger (Fig. 1). ML277 also reduces the latency and increases the amplitude of opening events from KCNE1-containing complexes (Figs. 2 and 3), although the amplitude increase is greatly diminished in channels with a 4:4 KCNE1:KCNQ1 stoichiometry (EQ). This amplitude change in the homomer is subtly different between channels locked in intermediate (IO) and fully activated (AO) open states (Fig. 5) that may be an amplification of differences in conductance that were too small to be seen in the absence of drug in our previous study (Hou et al., 2017). Overall, these results contrast with our observations of cAMP-dependent regulation of I_{Ks}, which resulted in more events at higher amplitudes but not openings beyond those seen in control (Thompson et al., 2017).

VSD gating versus pore effects

It was clear from the original studies of ML277 that there were multiple effects on the channel, with an increase in current being accompanied by changes to gating but also changes at the pore level in the form of a decreased Rb^+ to K^+ conductance (G_{Rb}/G_K) ratio (Xu et al., 2015). Two lines of evidence in particular suggested that we might see a change in KCNQ1 pore function upon ML277 treatment. Previous work had shown that low-dose ML277 could increase KCNQ1 currents without affecting VSD gating when monitored by voltage-clamp fluorometry (Hou et al., 2019). This same study using the R4 mutant showed an increase in current on ML277 treatment. Obviously, if the channel is already activated and the VSDs fixed, as in the case of R2 and R4, any increase in current must result from drug-induced changes in VSD–pore coupling that favor/stabilize pore opening, increased conductance, or reduced inactivation.

In this study, we have two measures for increases in current induced by ML277. These are the relative change in whole-cell

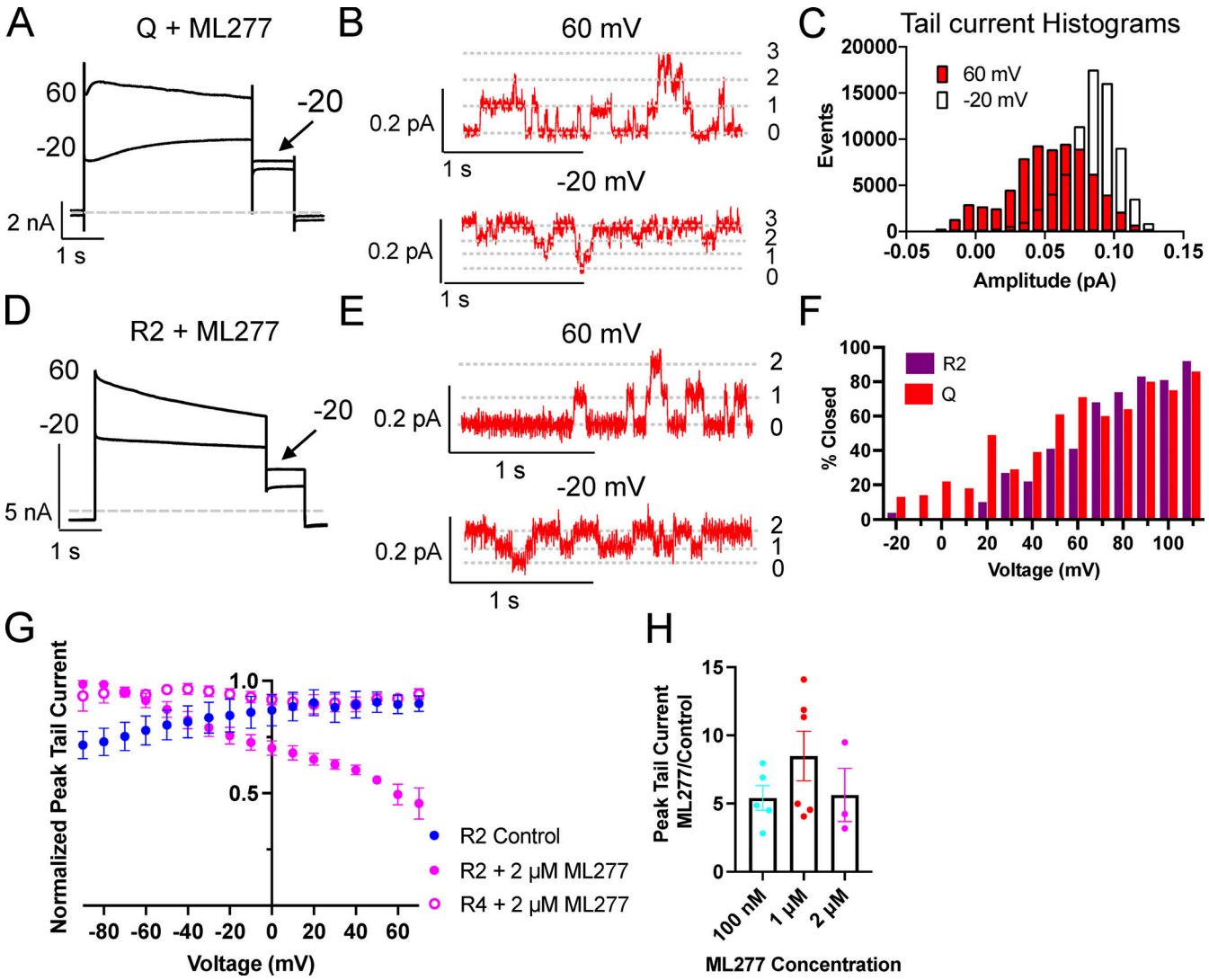

Figure 7. **Open probability of ML277 activated KCNQ1 and R2 channels decrease with voltage. (A)** Representative whole-cell currents of KCNQ1 obtained during a voltage-clamp protocol after 1 μM ML277 treatment. Cells were held at −90 and pulsed from −90 to +60 or +100 in 10-mV steps for 4 s, then to −40 mV for 0.9 s. The interpulse interval was 15 s. Only the −20 and 60 mV traces are shown for clarity. **(B)** Representative portions of cell-attached recordings of a three-channel patch of KCNQ1 + ML277 at +60 mV (upper trace) and −20 mV (lower trace). **(C)** All-points amplitude histograms from the tail currents of the same cell-attached patch as in B. Histograms are for 10 traces at each test pulse. **(D)** Representative whole-cell currents of R2 after treatment with 2 μM ML277. Protocol as in A. Only −20 and +60 mV are shown for clarity. **(E)** Representative portions of cell-attached recordings of a two-channel patch of R2 + 1 μM ML277 at +60 mV (upper trace) and −20 mV (lower trace). **(F)** Percent closed time at each voltage for an approximately two-channel patch of R2 or KCNQ1. Same protocol as in A except HP was −80 mV. Only sweeps with at least one recognizable closing could be analyzed. **(G)** G-V plots of R2 before (n = 3) and after treatment with 2 μM ML277 (n = 3) and R4 after treatment with 2 μM ML277 (n = 5). Protocol as in A. **(H)** Bar chart showing the tail current amplitude in ML277 divided by control amplitude for KCNQ1 in different concentrations of ML277. All error bars denote mean ± SEM.

tail current induced by the drug, and the increase in single-channel opening amplitudes. KCNQ1 showed an 8.4-fold mean increase in tail currents, with some cells showing up to a 12- or 14-fold increase (Fig. 2 B and Fig. S1 D), while the amplitude of KCNQ1 openings alone increased approximately threefold from ∼0.022 pA at +60 mV to 0.069 pA in ML277 (Fig. 1 G and Fig. 5 E). Removal of the ability of the VSD to influence the action of ML277 still resulted in ∼3.5- and 6-fold increases in tail current amplitudes, and 3-fold increases in single-channel amplitudes for R2 and R4, respectively (Fig. 4), and about 3-fold increases in tail currents in channels made up of E160R-Q* (Fig. 6 B). As more active VSDs are included in E160R-Q* channels, and the ML277 action on the VSD is added in, the drug effect on the tail current increases in a step-wise fashion. Together with the dose dependence of the gating effects of E160R mutants (Fig. 6, C and D; and Fig. S2), this suggests that more than one ML277 can bind to each channel, and with each that is bound, a further current increase is possible.

Since WT channels are subject to ML277-induced changes in VSD and pore function, while R2, R4, and E160R-Q* are arguably only subject to pore effects of ML277, the ratios discussed above suggest that pore effects are at least an equally important contributor as VSD effects to the increase in current observed as a result of ML277 treatment. That we observed current decline

over time, particularly with EQ (Fig. 2 A and Fig. S1 A), and that ML277 did not increase the number of active sweeps suggested that ML277 might not act as a general PIP2 mimetic. As well, in the E160R-Q* channel with four copies of the E160R mutant (Fig. 6, A and B), the VSDs are held at rest, and thus any ion conduction is the result of spontaneous PD opening with minimal involvement from VSD coupling. Enhancement by ML277 would then result from spontaneous openings, longer openings, bigger openings due to enhanced conductance, or a combination of these, whether by direct binding to the channel or by affecting other modulators such as PIP2 or calmodulin. We did try some single-channel recordings of this mutant in the hope of capturing these events but were not successful.

The decoupled channel and resting KCNQ1 conductance

KCNQ1 is said to have "loose coupling" between the VSD and the PD (Vardanyan and Pongs, 2012). This can manifest in channels that have activated VSDs and a closed pore due to depleted PIP2 (Zaydman et al., 2013; Barro-Soria et al., 2017, Sun and MacKinnon, 2017, 2020) and also as channels conducting (voltage-independent conductance fraction) at voltages at which the VSD is in the resting state (Ma et al., 2011; Barro-Soria et al., 2014; Osteen et al., 2012; Zaydman et al., 2014). It is either this small probability event affected by ML277 that results in the small increase in currents in cells expressing E160R-Q* (Fig. 6, A and B), or perhaps ML277 itself is acting as a ligand to open the channel. How KCNQ1 is able to conduct with a VSD at rest is potentially the result of several unique aspects of the channel. First, KCNQ1 lacks the Pro-Val-Pro motif that makes up the S6 gate in many other Kv channels (Seebohm et al., 2006), and this makes the KCNQ1 pore more stable in the open state (Vardanyan and Pongs, 2012), with many mutations in KCNQ1 leading to constitutive currents (Ma et al., 2011). Second, the S4-S5L that connects the VSD to the pore contains a loop structure at the N terminus where other Kv channels have a longer α helix (Sun and MacKinnon, 2017). This flexible loop, with two sequential glycines, might also allow for less rigid coupling between the VSD and the pore. Third, KCNQ1 is also a ligand gated channel, with both PIP2 and calcium via calmodulin being critical to KCNQ1 pore opening (Ghosh et al., 2006; Shamgar et al., 2006; Chang et al., 2018).

KCNQ1 inactivation and ML277

Inactivation of KCNQ1 is time- and voltage-dependent, requiring depolarizations above −30 mV for >100 ms to become evident as a hook in the tail currents, which reflects a faster recovery process compared with the rate of deactivation (Sanguinetti et al., 1996; Tristani-Firouzi and Sanguinetti, 1998). This inactivated state is not absorbing and reaches a steady-state >40 mV (Pusch et al., 1998). It is not sensitive to changes in external potassium concentration, which differentiates it from classical C-type inactivation (Tristani-Firouzi and Sanguinetti, 1998). The delay in reaching the inactivated state and the presence of the hook in the tail current, in addition to a progressive slowing of deactivation as depolarization is prolonged, led to the conclusion that KCNQ1 has at least two open states. This notion of more than one open state was further supported by studies that showed the second open state was more sensitive to Na^+ block (Pusch et al., 2001). More recently, it has been suggested that KCNQ1 is not inactivating per se, but that current decline is a result of occupancy of a second open state with a lower open probability (Hou et al., 2017). ML277 is thought to eliminate inactivation as no hook was observed in the tail currents after drug exposure (Yu et al., 2013). What, then, is the nature of the current and/or conductance decline at higher voltages in KCNQ1 and R2 (Figs. 1, 4, and 7)? This could result from several ML277-related actions. Voltage-dependent effects on drug affinity could lead to a reduction in drug potency. Alternatively, ML277 might induce or enhance a secondary slow inactivation process independent from the generally recognized relatively fast inactivation seen in KCNQ1. Non–drug-related effects, such as voltage-dependent intracellular Na^+ block of the open pore at positive potentials, might also be revealed by ML277 exposure (Pusch et al., 2001).

There are many interesting links between inactivation and ML277. For example, KCNQ2, which does not inactivate (Seebohm et al., 2001; Jensen et al., 2007) and has a low G_{Rb}/G_K ratio (Prole and Marrion, 2004), is insensitive to ML277 (Mattmann et al., 2012). Swapping the glycine at 272 in KCNQ1 for cysteine, which is the equivalent residue in KCNQ2, abolishes inactivation in KCNQ1 and reduces the G_{Rb}/G_K ratio (Seebohm et al., 2001; Seebohm et al., 2003), and while ML277 has not reportedly been used on G272C, G272A is less sensitive to the drug (Hou et al., 2020). G272 is within 4 Å of F332 in the KCNQ1 cryo-EM structure (6UZZ; Sun and MacKinnon, 2020), and when this residue is mutated, F332A, the effects of ML277 are reduced (Xu et al., 2015), and inactivation is again removed (Seebohm et al. 2003). It is difficult to tell if residues in this region of the channel make up the binding site for ML277 or they are important to the mechanism of action of the drug, but it is thought that perhaps flexibility at this location is important for modulation by KCNE1 (Nakajo et al. 2011), an interaction that would also explain the decreased effect of ML277, the loss of inactivation, and the reduction of G_{Rb}/G_K on KCNE1 coexpression, whether sterically or allosterically.

Next to G272 is another residue of interest in the inactivation story. L273, which appears to interact with the pore helix at G306 and V307 (Sun and MacKinnon, 2020), when mutated to L273F introduces an additional slow inactivation process into KCNQ1 (Gibor et al., 2007; Seebohm et al., 2001). While several different mutations spread between the S4-S6 region have been shown to lead to a slow inactivation process, that this site is next to G272 could be relevant to ML277's effects on inactivation. Slow inactivation of R2 could explain why R4 showed larger increases in tail currents over control (Fig. 5 C), while having smaller single-channel openings than R2 upon ML277 treatment (Fig. 5 E). Of particular interest is that KCNQ1 seems to share this "slow inactivation" characteristic with R2 (Fig. 7, A–C and H), in addition to having larger single-channel openings (Fig. 5 I). Together this suggests that the KCNQ1 VSD may largely transition only to the IO state and not the AO state. This could explain the greater overlap of the fluorescence-voltage and G-V curves (Osteen et al., 2010) and the greater sensitivity to the blocker XE991 (Taylor et al., 2020).

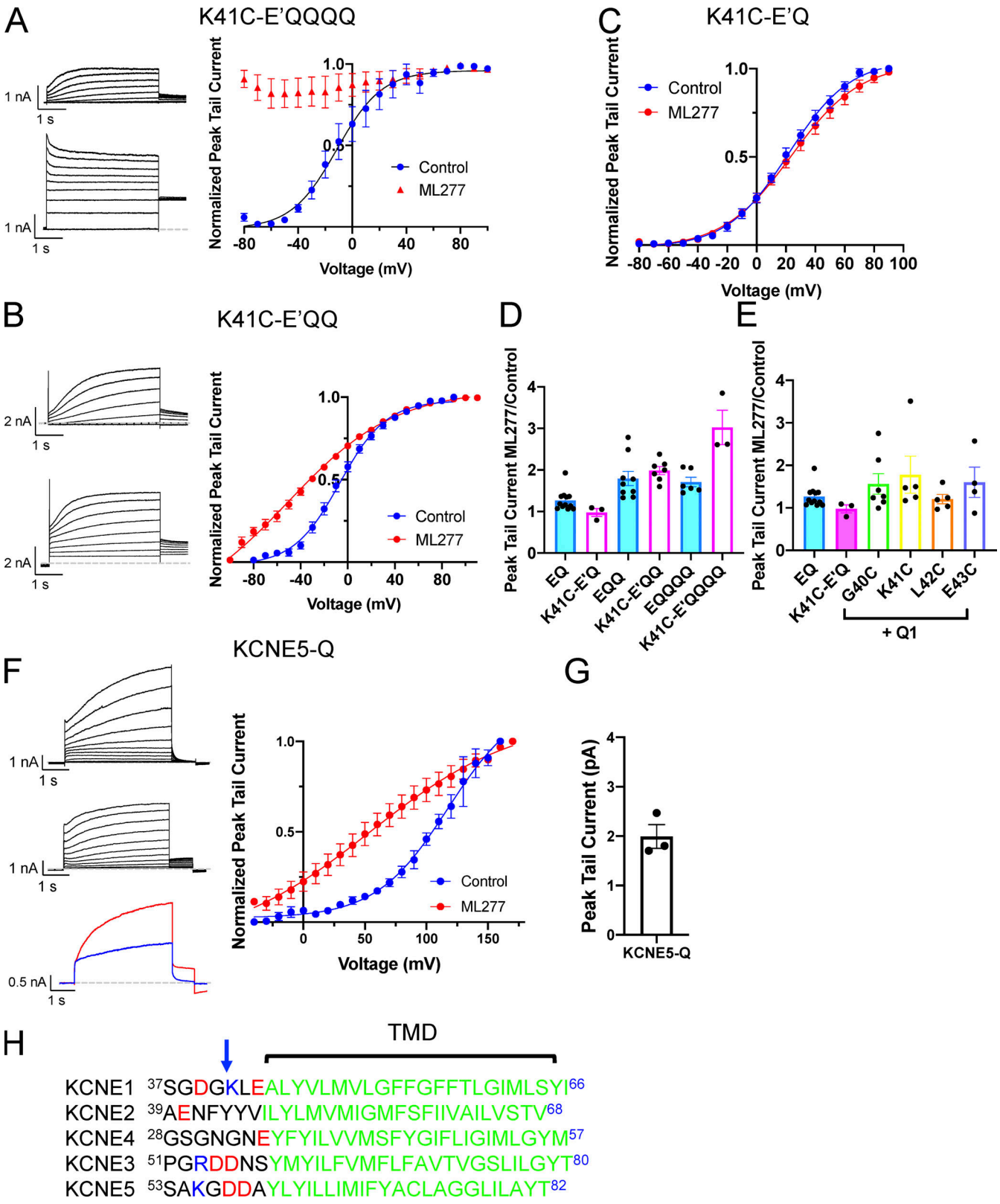

Figure 8. **The K41C mutation in KCNE1 allows ML277 to activate I_{Ks} as long as the complexes are not fully saturated. (A)** Representative whole-cell currents of K41C-E'QQQQ obtained using a voltage-clamp protocol before (top) and after 1 µM ML277 (bottom). Cells were held at −90 and pulsed from −90 to +100 in 10-mV steps for 4 s, then to −40 mV for 0.9 s. The interpulse interval was 15 s. Only even voltages are shown for clarity. The graph on the right shows the G-V plots (n = 3). **(B)** Representative whole-cell currents of K41C-E'QQ obtained using the same activation protocol as described in A. The upper record is before ML277, and the lower trace is after 1 µM ML277 was added to the bath. The graph on the right shows the G-V plots (n = 4 or 5). **(C)** G-V plots for K41C-E'Q in control conditions and in 1 µM ML277 (n = 4 or 5). **(D)** Bar chart shows the tail current amplitude in ML277 divided by control amplitude for WT channel

complexes and those containing the K41C-KCNE1 mutant with different stoichiometries of E1:Q1. **(E)** Bar chart showing the tail current amplitude in ML277 divided by control amplitude for WT I_{Ks} and I_{Ks} assembled with various mutants of KCNE1. EQ and K41C-E'Q are linked constructs, and the others are co-transfected. **(F)** Representative whole-cell currents of KCNE5-Q obtained using the same activation protocol as described in A. The upper record is before ML277, and the middle record is after 1 µM ML277 was added to the bath. The lower panel shows a sample control trace (blue) and a trace collected in the presence of ML277. The cell was held at −90 mV, pulsed to +60 mV for 4 s, and then −40 mV for 0.8 s. The interpulse interval was 15 s. The graph on the right shows the G-V plots (n = 4). **(G)** Bar chart showing ratio of the tail current for KCNE5-Q in ML277 divided by control after a test pulse to 60 mV for 4 s. **(H)** Sequence alignment of human KCNE proteins for the TMD region and that just N-terminal to it. Arrow indicates K41 in KCNE1. All error bars denote mean ± SEM.

Stoichiometry in cardiomyocytes

As mentioned previously, an important aim of the study of fixed stoichiometries of I_{Ks} is to enable better interpretation of cardiomyocyte data. ML277 has been shown to shorten the action potential in human cardiac iPSCs (Yu et al., 2013), guinea pig and canine ventricular myocytes (Xu et al., 2015), and rabbit atrial myocytes (Kanaporis et al., 2019). This action potential shortening was accompanied by a 28% increase in I_{Ks} currents in guinea pig, ∼100% in human iPSCs, and 228% in canine ventricular myocytes (Xu et al., 2015), with no shift in the $V_{1/2}$ of activation in the guinea pig (remained at ∼25 mV) and a +30 mV shift in the canine cells (shifting from approximately −10 to +20 mV). In rabbit atrial myocytes, ML277 treatment resulted in an ∼50% increase in K^+ currents and an approximately −10 mV shift in the $V_{1/2}$ (Kanaporis et al., 2019). These data suggest that in the guinea pig, I_{Ks} might be saturated with KCNE1 (reflecting our EQ data; Fig. 2, B and C), but that in the iPSCs, rabbit and the canine myocytes either 1:4 or 2:4 are possible, though we did not see a positive shift in $V_{1/2}$ with any of our constructs (Fig. 2 and Table 1). The sequence for canine KCNQ1 is the most divergent of the four species above, showing 71% identity with human KCNQ1, which increases to 94% when just considering the region from the start of S1 to the end of S6. Much of the divergence occurs in the lower S1 domain as well as an A149V in the S1-S2L, L187I in the S2-S3L, and V207L in S3, as well as an E290D and R293Q in the loop between S5 and the pore helix (numbering is as for human sequence). It is not obvious why these changes might reverse the effect on activation from that seen in the other three species, which have 99% identity between the start of S1 and the end of S6.

We and others have shown that the region just N-terminal to the TMD of KCNE1 is important for the effects of stilbenes such as 4,4'-diisothiocyano-2,2'-stilbenedisulfonic acid and 4-acetamido-4'-isothiocyanatostilbene-2,2'-disulfonic acid, and fenamates such as MefA (Abitbol et al., 1999; Wang et al., 2020), on I_{Ks} currents. We also found that a K41C mutation in KCNE1 abolished the effects of MefA, which is most potent as an activator on a 4:4 KCNE1:KCNQ1 stoichiometry. In addition, a double mutant of KCNE1, G40N/K41N, when expressed with KCNQ1, showed enhanced rubidium ion (Rb^+) conductance halfway between that normally seen for I_{Ks} and KCNQ1 alone (Barro-Soria et al., 2017), indicating this region of KCNE1 was interacting with the PD and could affect conductance. Based on the KCNQ1/KCNE3 structure (Sun and MacKinnon, 2020), these residues would be expected to be near the external portion of the filter helix, and there are also species sequence divergences surrounding K41 in KCNE1. The human and guinea pig KCNE1 sequences are ^{40}GKLE^{43}, whereas the canine sequence is SQLA and the rabbit sequence is GQME, which presents another potential variable in the species response to ML277. We did test in particular whether the charge at K41 in human KCNE1 was important for reducing the effects of ML277 (Fig. 8), and if this might explain the results in rabbit and canine myocytes by using the K41C mutant that abolished the effect of MefA (Wang et al., 2020). Our results suggest that if I_{Ks} in the rabbit and canine were not saturated with KCNE1, it is possible that the loss of charge at position 41 of KCNE1 could be a contributing factor in the greater response to ML277 in these species. This is also consistent with the more gradual decline in the ML277 effect with increasing KCNE3 expression (Yu et al., 2013) that has the sequence ^{54}DDNS^{57} at this location, and the results showing a doubling of peak tail currents with a KCNE5-KCNQ1 construct (Fig. 8, F and G) that contains the sequence ^{56}GDDA^{59} (Fig. 8 H).

Do we know anything more about where ML277 is binding?

Studies that have tested ML277 on mutants of KCNQ1 have indicated an ML277 binding site in the vicinity of the S4-S5L and the lower S5 and S6 (Xu et al., 2015; Hou et al., 2020). Slowed deactivation and current-enhancing effects could even be separated by specific point mutations, one of these being a turn and a half of the helix below G272 (Xu et al., 2015). While we did not specifically explore this issue, we can add several additional observations from our experience. There do appear to be different effects depending on dose of ML277 (conductance versus gating). Whether this means two different binding sites with different affinities or one effect requires fewer bound ML277 molecules is not clear.

If the ML277 binding site extends to near where G40/K41 are found when KCNE1 is part of the complex, this would explain why ML277 enhances conductance, reduces Rb^+ permeation, and is less effective on the 4:4 stoichiometry (Xu et al., 2015), a result perhaps of some steric or electrostatic hindrance by the KCNE1 subunit. Looking at the cryo-EM structure, we cannot explain the observation that when ML277 was added to the bath after recording had started, it often took at least 10 min to start seeing the change in single-channel openings in KCNQ1, R2, and R4. However, if the bath was not cleaned properly between batches of cells, the change was immediately evident, suggesting that the patch pipette was hindering drug access to the binding site.

Two lines of evidence suggest that there may be a site of ML277 interaction of unknown significance in the vicinity of the inner vestibule. The first is the fact that HMR is less effective when ML277 is in the bath at the same time (Fig. S1 B), as though there is competition for a partially overlapping binding site, or the activator is providing steric hindrance to the blocker. The second is that the S338F mutant is actually blocked by ML277 (Fig. S3). The significance of this inner vestibule site is unclear but is not related to the changes in gating or enhanced current as these properties persist for many minutes after ML277 washout from the bath and restoration of full HMR block (Fig. S1 E).

Conclusions

ML277 has complex effects on KCNQ1 channels, leading to changes in both VSD gating behavior and pore activation, with each contributing equally to enhanced whole-cell currents. While the effects of ML277 are much more modest in the presence of KCNE1, the stoichiometry of I_{Ks} is unknown in the human heart and may well be variable, which might make some channel behavior modifiable by ML277 or its analogues. The slowed deactivation and a small boost in conductance might be enough to rescue some channel complexes containing LQT mutations, particularly at high heart rates.

Acknowledgments

Jeanne M. Nerbonne served as editor.

We thank Fariba Ataei and Dr. Emely Thompson for their technical assistance in cell culture (F. Ataei) and some data organization and analysis (E. Thompson).

This research was funded by the Natural Sciences and Engineering Research Council of Canada (grant no. RGPIN-2016-05422), the Canadian Institutes of Health Research (grant no. PJT-156181), and the Heart and Stroke Foundation of Canada (grant no. G17-0018392; all grants to D. Fedida).

The authors declare no competing financial interests.

Author contributions: J. Eldstrom: conceptualization, data acquisition, data analysis and interpretation, writing-original draft, writing-reviewing and editing. D.A. McAfee: data acquisition, reviewing and editing. Y. Dou: data acquisition. Y. Wang: data acquisition. D. Fedida: data interpretation, writing-reviewing and editing, funding acquisition.

Submitted: 19 May 2021
Revised: 16 July 2021
Accepted: 15 September 2021

References

Abitbol, I., A. Peretz, C. Lerche, A.E. Busch, and B. Attali. 1999. Stilbenes and fenamates rescue the loss of I_{KS} channel function induced by an LQT5 mutation and other IsK mutants. *EMBO J.* 18:4137–4148. https://doi.org/10.1093/emboj/18.15.4137

Barhanin, J., F. Lesage, E. Guillemare, M. Fink, M. Lazdunski, and G. Romey. 1996. K_VLQT1 and lsK (minK) proteins associate to form the I_{Ks} cardiac potassium current. *Nature.* 384:78–80. https://doi.org/10.1038/384078a0

Barro-Soria, R., S. Rebolledo, S.I. Liin, M.E. Perez, K.J. Sampson, R.S. Kass, and H.P. Larsson. 2014. KCNE1 divides the voltage sensor movement in KCNQ1/KCNE1 channels into two steps. *Nat. Commun.* 5:3750. https://doi.org/10.1038/ncomms4750

Barro-Soria, R., R. Ramentol, S.I. Liin, M.E. Perez, R.S. Kass, and H.P. Larsson. 2017. KCNE1 and KCNE3 modulate KCNQ1 channels by affecting different gating transitions. *Proc. Natl. Acad. Sci. USA.* 114:E7367–E7376. https://doi.org/10.1073/pnas.1710335114

Busch, A.E., G.L. Busch, E. Ford, H. Suessbrich, H.J. Lang, R. Greger, K. Kunzelmann, B. Attali, and W. Stühmer. 1997. The role of the IsK protein in the specific pharmacological properties of the IKs channel complex. *Br. J. Pharmacol.* 122:187–189. https://doi.org/10.1038/sj.bjp.0701434

Chang, A., F. Abderemane-Ali, G.L. Hura, N.D. Rossen, R.E. Gate, and D.L. Minor Jr. 2018. A Calmodulin C-Lobe Ca^{2+}-Dependent Switch Governs Kv7 Channel Function. *Neuron.* 97:836–852.e6. https://doi.org/10.1016/j.neuron.2018.01.035

Eldstrom, J., Z. Wang, D. Werry, N. Wong, and D. Fedida. 2015. Microscopic mechanisms for long QT syndrome type 1 revealed by single-channel analysis of I_{Ks} with S3 domain mutations in KCNQ1. *Heart Rhythm.* 12:386–394. https://doi.org/10.1016/j.hrthm.2014.10.029

Gao, Z., Q. Xiong, H. Sun, and M. Li. 2008. Desensitization of chemical activation by auxiliary subunits: convergence of molecular determinants critical for augmenting KCNQ1 potassium channels. *J. Biol. Chem.* 283:22649–22658. https://doi.org/10.1074/jbc.M802426200

Ghosh, S., D.A. Nunziato, and G.S. Pitt. 2006. KCNQ1 assembly and function is blocked by long-QT syndrome mutations that disrupt interaction with calmodulin. *Circ. Res.* 98:1048–1054. https://doi.org/10.1161/01.RES.0000218863.44140.f2

Gibor, G., D. Yakubovich, A. Rosenhouse-Dantsker, A. Peretz, H. Schottelndreier, G. Seebohm, N. Dascal, D.E. Logothetis, Y. Paas, and B. Attali. 2007. An inactivation gate in the selectivity filter of KCNQ1 potassium channels. *Biophys. J.* 93:4159–4172. https://doi.org/10.1529/biophysj.107.107987

Hou, P., J. Eldstrom, J. Shi, L. Zhong, K. McFarland, Y. Gao, D. Fedida, and J. Cui. 2017. Inactivation of KCNQ1 potassium channels reveals dynamic coupling between voltage sensing and pore opening. *Nat. Commun.* 8:1730. https://doi.org/10.1038/s41467-017-01911-8

Hou, P., J. Shi, K.M. White, Y. Gao, and J. Cui. 2019. ML277 specifically enhances the fully activated open state of KCNQ1 by modulating VSD-pore coupling. *eLife.* 8:e48576. https://doi.org/10.7554/eLife.48576

Hou, P., P.W. Kang, A.D. Kongmeneck, N.D. Yang, Y. Liu, J. Shi, X. Xu, K.M. White, M.A. Zaydman, M.A. Kasimova, et al. 2020. Two-stage electromechanical coupling of a K_V channel in voltage-dependent activation. *Nat. Commun.* 11:676. https://doi.org/10.1038/s41467-020-14406-w

Jensen, H.S., M. Grunnet, and S.P. Olesen. 2007. Inactivation as a new regulatory mechanism for neuronal Kv7 channels. *Biophys. J.* 92:2747–2756. https://doi.org/10.1529/biophysj.106.101287

Kanaporis, G., Z.M. Kalik, and L.A. Blatter. 2019. Action potential shortening rescues atrial calcium alternans. *J. Physiol.* 597:723–740. https://doi.org/10.1113/JP277188

Li, Y., M.A. Zaydman, D. Wu, J. Shi, M. Guan, B. Virgin-Downey, and J. Cui. 2011. KCNE1 enhances phosphatidylinositol 4,5-bisphosphate (PIP2) sensitivity of IKs to modulate channel activity. *Proc. Natl. Acad. Sci. USA.* 108:9095–9100. https://doi.org/10.1073/pnas.1100872108

Liin, S.I., R. Barro-Soria, and H.P. Larsson. 2015. The KCNQ1 channel - remarkable flexibility in gating allows for functional versatility. *J. Physiol.* 593:2605–2615. https://doi.org/10.1113/jphysiol.2014.287607

Liu, L., F. Wang, H. Lu, X. Ren, and J. Zou. 2014. Chromanol 293B, an inhibitor of KCNQ1 channels, enhances glucose-stimulated insulin secretion and increases glucagon-like peptide-1 level in mice. *Islets.* 6:e962386. https://doi.org/10.4161/19382014.2014.962386

Loussouarn, G., K.H. Park, C. Bellocq, I. Baró, F. Charpentier, and D. Escande. 2003. Phosphatidylinositol-4,5-bisphosphate, PIP2, controls KCNQ1/KCNE1 voltage-gated potassium channels: a functional homology between voltage-gated and inward rectifier K+ channels. *EMBO J.* 22:5412–5421. https://doi.org/10.1093/emboj/cdg526

Ma, L.J., I. Ohmert, and V. Vardanyan. 2011. Allosteric features of KCNQ1 gating revealed by alanine scanning mutagenesis. *Biophys. J.* 100:885–894. https://doi.org/10.1016/j.bpj.2010.12.3726

Ma, D., H. Wei, J. Lu, D. Huang, Z. Liu, L.J. Loh, O. Islam, R. Liew, W. Shim, and S.A. Cook. 2015. Characterization of a novel KCNQ1 mutation for type 1 long QT syndrome and assessment of the therapeutic potential of a novel IKs activator using patient-specific induced pluripotent stem cell-derived cardiomyocytes. *Stem Cell Res. Ther.* 6:39. https://doi.org/10.1186/s13287-015-0027-z

Mattmann, M.E., H. Yu, Z. Lin, K. Xu, X. Huang, S. Long, M. Wu, O.B. McManus, D.W. Engers, U.M. Le, et al. 2012. Identification of (R)-N-(4-(4-methoxyphenyl)thiazol-2-yl)-1-tosylpiperidine-2-carboxamide, ML277, as a novel, potent and selective K(v)7.1 (KCNQ1) potassium channel activator. *Bioorg. Med. Chem. Lett.* 22:5936–5941. https://doi.org/10.1016/j.bmcl.2012.07.060

Mruk, K., and W.R. Kobertz. 2009. Discovery of a novel activator of KCNQ1-KCNE1 K channel complexes. *PLoS One.* 4:e4236. https://doi.org/10.1371/journal.pone.0004236

Murray, C.I., M. Westhoff, J. Eldstrom, E. Thompson, R. Emes, and D. Fedida. 2016. Unnatural amino acid photo-crosslinking of the IKs channel complex demonstrates a KCNE1:KCNQ1 stoichiometry of up to 4:4. *eLife.* 5:e11815. https://doi.org/10.7554/eLife.11815

Nakajo, K., A. Nishino, Y. Okamura, and Y. Kubo. 2011. KCNQ1 subdomains involved in KCNE modulation revealed by an invertebrate KCNQ1 orthologue. *J. Gen. Physiol.* 138:521–535. https://doi.org/10.1085/jgp.201110677

Osteen, J.D., C. Gonzalez, K.J. Sampson, V. Iyer, S. Rebolledo, H.P. Larsson, and R.S. Kass. 2010. KCNE1 alters the voltage sensor movements

necessary to open the KCNQ1 channel gate. *Proc. Natl. Acad. Sci. USA.* 107:22710–22715. https://doi.org/10.1073/pnas.1016300108

Osteen, J.D., R. Barro-Soria, S. Robey, K.J. Sampson, R.S. Kass, and H.P. Larsson. 2012. Allosteric gating mechanism underlies the flexible gating of KCNQ1 potassium channels. *Proc. Natl. Acad. Sci. USA.* 109:7103–7108. https://doi.org/10.1073/pnas.1201582109

Prole, D.L., and N.V. Marrion. 2004. Ionic permeation and conduction properties of neuronal KCNQ2/KCNQ3 potassium channels. *Biophys. J.* 86:1454–1469. https://doi.org/10.1016/S0006-3495(04)74214-9

Pusch, M., R. Magrassi, B. Wollnik, and F. Conti. 1998. Activation and inactivation of homomeric KvLQT1 potassium channels. *Biophys. J.* 75: 785–792. https://doi.org/10.1016/S0006-3495(98)77568-X

Pusch, M., L. Ferrera, and T. Friedrich. 2001. Two open states and rate-limiting gating steps revealed by intracellular Na^+ block of human KCNQ1 and KCNQ1/KCNE1 K^+ channels. *J. Physiol.* 533:135–143. https://doi.org/10.1111/j.1469-7793.2001.0135b.x

Salata, J.J., N.K. Jurkiewicz, J. Wang, B.E. Evans, H.T. Orme, and M.C. Sanguinetti. 1998. A novel benzodiazepine that activates cardiac slow delayed rectifier K+ currents. *Mol. Pharmacol.* 54:220–230. https://doi.org/10.1124/mol.54.1.220

Sanguinetti, M.C., M.E. Curran, A. Zou, J. Shen, P.S. Spector, D.L. Atkinson, and M.T. Keating. 1996. Coassembly of K_VLQT1 and minK (IsK) proteins to form cardiac I_{Ks} potassium channel. *Nature.* 384:80–83. https://doi.org/10.1038/384080a0

Schwartz, P.J., M.J. Ackerman, C. Antzelevitch, C.R. Bezzina, M. Borggrefe, B.F. Cuneo, and A.A.M. Wilde. 2020. Inherited cardiac arrhythmias. *Nat. Rev. Dis. Primers.* 6:58. https://doi.org/10.1038/s41572-020-0188-7

Seebohm, G., C.R. Scherer, A.E. Busch, and C. Lerche. 2001. Identification of specific pore residues mediating KCNQ1 inactivation. A novel mechanism for long QT syndrome. *J. Biol. Chem.* 276:13600–13605. https://doi.org/10.1074/jbc.M008373200

Seebohm, G., M.C. Sanguinetti, and M. Pusch. 2003. Tight coupling of rubidium conductance and inactivation in human KCNQ1 potassium channels. *J. Physiol.* 552:369–378. https://doi.org/10.1113/jphysiol.2003.046490

Seebohm, G., N. Strutz-Seebohm, O.N. Ureche, R. Baltaev, A. Lampert, G. Kornichuk, K. Kamiya, T.V. Wuttke, H. Lerche, M.C. Sanguinetti, and F. Lang. 2006. Differential roles of S6 domain hinges in the gating of KCNQ potassium channels. *Biophys. J.* 90:2235–2244. https://doi.org/10.1529/biophysj.105.067165

Shamgar, L., L. Ma, N. Schmitt, Y. Haitin, A. Peretz, R. Wiener, J. Hirsch, O. Pongs, and B. Attali. 2006. Calmodulin is essential for cardiac IKS channel gating and assembly: impaired function in long-QT mutations. *Circ. Res.* 98:1055–1063. https://doi.org/10.1161/01.RES.0000218979.40770.69

Sun, J., and R. MacKinnon. 2017. Cryo-EM Structure of a KCNQ1/CaM Complex Reveals Insights into Congenital Long QT Syndrome. *Cell.* 169: 1042–1050.e9. https://doi.org/10.1016/j.cell.2017.05.019

Sun, J., and R. MacKinnon. 2020. Structural Basis of Human KCNQ1 Modulation and Gating. *Cell.* 180:340–347.e9. https://doi.org/10.1016/j.cell.2019.12.003

Taylor, K.C., P.W. Kang, P. Hou, N.D. Yang, G. Kuenze, J.A. Smith, J. Shi, H. Huang, K.M. White, D. Peng, et al. 2020. Structure and physiological function of the human KCNQ1 channel voltage sensor intermediate state. *eLife.* 9:e53901. https://doi.org/10.7554/eLife.53901

Thompson, E., J. Eldstrom, M. Westhoff, D. McAfee, E. Balse, and D. Fedida. 2017. cAMP-dependent regulation of I_{Ks} single-channel kinetics. *J. Gen. Physiol.* 149:781–798. https://doi.org/10.1085/jgp.201611734

Tristani-Firouzi, M., and M.C. Sanguinetti. 1998. Voltage-dependent inactivation of the human K+ channel KvLQT1 is eliminated by association with minimal K+ channel (minK) subunits. *J. Physiol.* 510:37–45. https://doi.org/10.1111/j.1469-7793.1998.037bz.x

Vardanyan, V., and O. Pongs. 2012. Coupling of voltage-sensors to the channel pore: a comparative view. *Front. Pharmacol.* 3:145. https://doi.org/10.3389/fphar.2012.00145

Wang, Y., J. Eldstrom, and D. Fedida. 2020. The I_{Ks} Ion Channel Activator Mefenamic Acid Requires KCNE1 and Modulates Channel Gating in a Subunit-Dependent Manner. *Mol. Pharmacol.* 97:132–144. https://doi.org/10.1124/mol.119.117952

Werry, D., J. Eldstrom, Z. Wang, and D. Fedida. 2013. Single-channel basis for the slow activation of the repolarizing cardiac potassium current, I_{Ks}. *Proc. Natl. Acad. Sci. USA.* 110:E996–E1005. https://doi.org/10.1073/pnas.1214875110

Westhoff, M., C.I. Murray, J. Eldstrom, and D. Fedida. 2017. Photo-Cross-Linking of I_{Ks} Demonstrates State-Dependent Interactions between KCNE1 and KCNQ1. *Biophys. J.* 113:415–425. https://doi.org/10.1016/j.bpj.2017.06.005

Westhoff, M., J. Eldstrom, C.I. Murray, E. Thompson, and D. Fedida. 2019. I_{Ks} ion-channel pore conductance can result from individual voltage sensor movements. *Proc. Natl. Acad. Sci. USA.* 116:7879–7888. https://doi.org/10.1073/pnas.1811623116

Wuriyanghai, Y., T. Makiyama, K. Sasaki, T. Kamakura, Y. Yamamoto, M. Hayano, T. Harita, S. Nishiuchi, J. Chen, H. Kohjitani, et al. 2018. Complex aberrant splicing in the induced pluripotent stem cell-derived cardiomyocytes from a patient with long QT syndrome carrying KCNQ1-A344Aspl mutation. *Heart Rhythm.* 15:1566–1574. https://doi.org/10.1016/j.hrthm.2018.05.028

Xu, Y., Y. Wang, M. Zhang, M. Jiang, A. Rosenhouse-Dantsker, T. Wassenaar, and G.N. Tseng. 2015. Probing binding sites and mechanisms of action of an I(Ks) activator by computations and experiments. *Biophys. J.* 108: 62–75. https://doi.org/10.1016/j.bpj.2014.10.059

Yu, H., Z. Lin, M.E. Mattmann, B. Zou, C. Terrenoire, H. Zhang, M. Wu, O.B. McManus, R.S. Kass, C.W. Lindsley, et al. 2013. Dynamic subunit stoichiometry confers a progressive continuum of pharmacological sensitivity by KCNQ potassium channels. *Proc. Natl. Acad. Sci. USA.* 110: 8732–8737. https://doi.org/10.1073/pnas.1300684110

Zaydman, M.A., J.R. Silva, K. Delaloye, Y. Li, H. Liang, H.P. Larsson, J. Shi, and J. Cui. 2013. Kv7.1 ion channels require a lipid to couple voltage sensing to pore opening. *Proc. Natl. Acad. Sci. USA.* 110:13180–13185. https://doi.org/10.1073/pnas.1305167110

Zaydman, M.A., M.A. Kasimova, K. McFarland, Z. Beller, P. Hou, H.E. Kinser, H. Liang, G. Zhang, J. Shi, M. Tarek, and J. Cui. 2014. Domain-domain interactions determine the gating, permeation, pharmacology, and subunit modulation of the IKs ion channel. *eLife.* 3:e03606. https://doi.org/10.7554/eLife.03606

Zheng, Y., X. Zhu, P. Zhou, X. Lan, H. Xu, M. Li, and Z. Gao. 2012. Hexachlorophene is a potent KCNQ1/KCNE1 potassium channel activator which rescues LQTs mutants. *PLoS One.* 7:e51820. https://doi.org/10.1371/journal.pone.0051820

Supplemental material

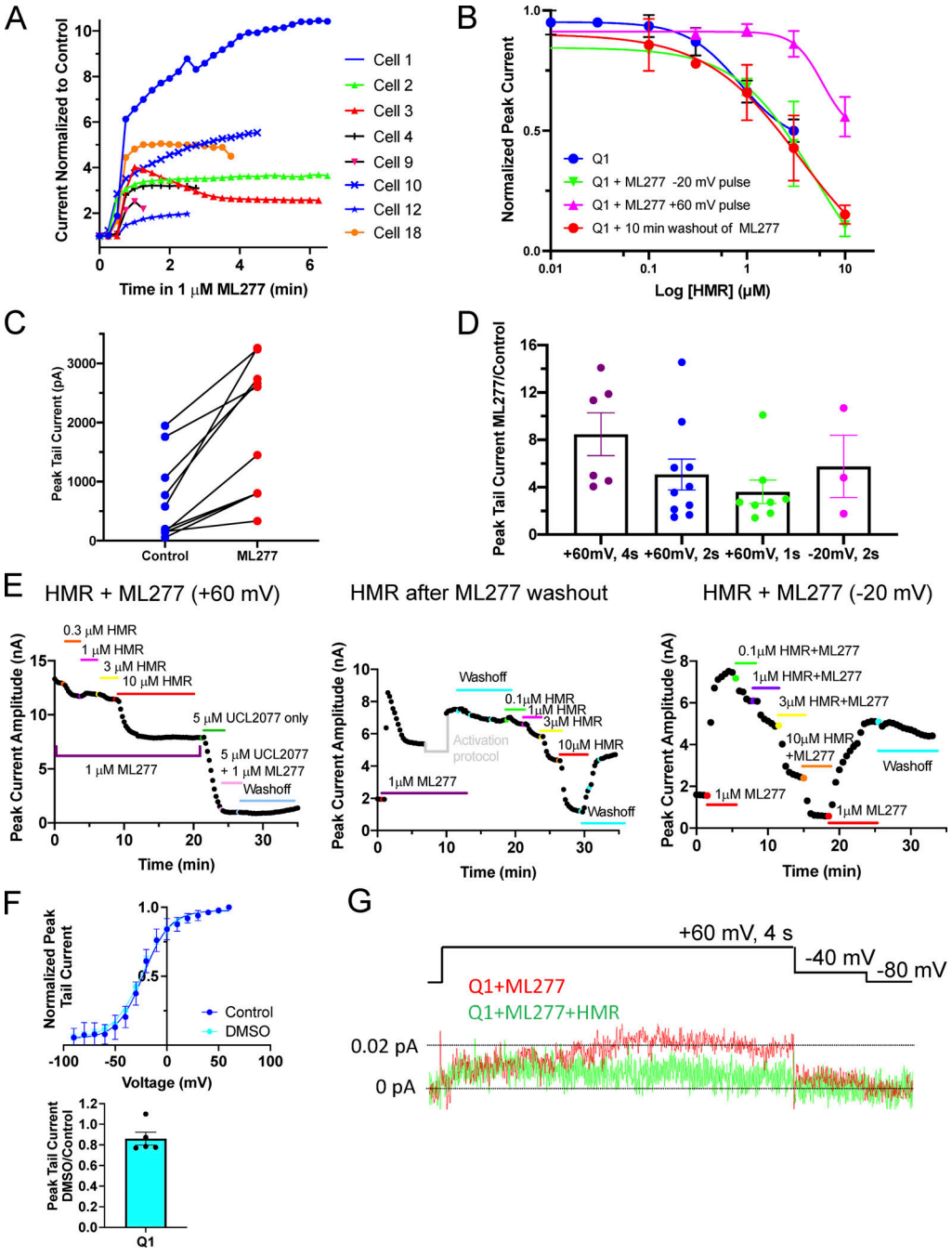

Figure S1. **Peak KCNQ1 currents after ML277 addition and response to HMR. (A)** Diary plots of peak KCNQ1 current over time after 1 μM ML277 addition, normalized to last control level for eight different cells. Cells were held at −80 mV and pulsed to +60 mV for 2 s, then to −40 mV for 1 s repeatedly with an interpulse interval of 15 s. In a few examples (red triangles, yellow circles), after ML277 has its effect, the current begins to decrease again before stabilizing, and while the decrease did not always happen in the recording time frame, it suggests that ML277 might not act as a PIP2 mimetic given that PIP2 has previously been shown to prevent rundown of whole-cell currents (Li et al., 2011; Loussouarn et al., 2003). **(B)** Concentration-response curves for HMR inhibition of KCNQ1 currents under different experimental conditions; KCNQ1 pulsed to +60 mV and HMR added after washout of ML277 (red circles, IC_{50} = 3.44 μM); KCNQ1 pulsed to +60 mV and HMR added with ML277 remaining in solution (magenta triangles, IC_{50} = 5.88 μM); KCNQ1 pulsed to −20 mV and HMR added with ML277 remaining in solution (green triangles, IC_{50} = 4.86 μM); and KCNQ1 in control bath solution pulsed to +60 mV (blue circles, IC_{50} = 2.54 μM), n = 2–6. **(C)** Paired peak tail current amplitudes before and after exposure to 1 μM ML277. Protocol was as in A. **(D)** Chart of peak KCNQ1 tail current amplitudes in ML277 divided by peak current in control conditions with four different test protocols as labeled. **(E)** Diary plots of KCNQ1 peak currents showing response to increasing concentrations of HMR under the different experimental conditions detailed in B. A pause in the diary plot is shown where a voltage-clamp protocol was run before beginning the 10-min washout. **(F)** Top: G-V plot of KCNQ1 before (blue circles) and after exposure to 0.1% DMSO (cyan circles). $V_{1/2}$ of activation and slope values was −22.5 ± 1.5 mV and 12.8 ± 2.0 for control, −23.7 ± 1.8 mV and 14.5 ± 1.8 in DMSO, n = 4 for each. Cells were held at −90 mV and pulsed from −90 to +80 for 4 s, then to −40 mV for 0.9 s, with an interpulse interval of 15 s. Bottom: Plot of peak tail currents in 0.1% DMSO divided by control values after a 4-s, +60 mV pulse. **(G)** Ensemble averages of 53 sweeps of KCNQ1 treated with 1 μM ML277 (red) and 53 sweeps of the same cell after treatment with 20 μM HMR. Protocol is shown above. The interpulse interval was 10 s. All error bars in the figure denote mean ± SEM.

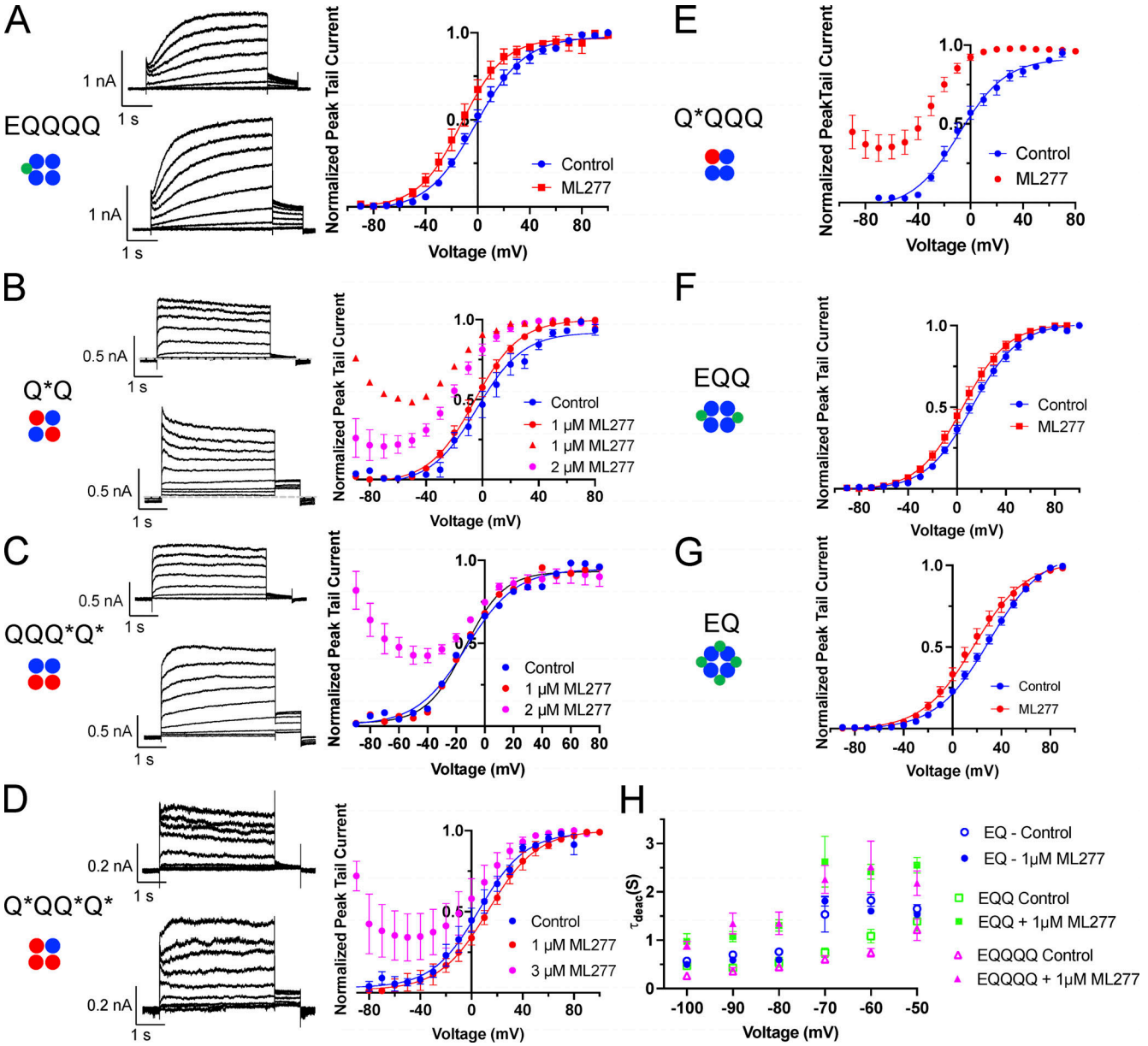

Figure S2. **G-V plots and some representative currents for EQQQQ, EQQ, EQ, and KCNQ1 E160R mutants before and after ML277 treatment.** Cartoons below construct labels denote the number and location of subunits in the channel tetramer containing WT (blue circle) or E160R containing KCNQ1 subunits (red circle) or KCNE1 (green circle). **(A)** Representative whole-cell currents of EQQQQ obtained using an activation protocol before (top) and after 1 μM ML277 (bottom). Cell was pulsed from a holding potential of −80 mV to +60 mV for 4 s, then for 1 s to −40 mV. The interpulse interval was 15 s. Right: G-V plots of EQQQQ before (blue circles) and after (red circles) 1 μM ML277 exposure. **(B–D)** Representative whole-cell currents of E160R-Q*Q (B), E160R-QQQ*Q* (C), and E160R-Q*QQ*Q* (D) obtained using an activation protocol before (top) and after 1 μM ML277 (bottom). Cells were held at −90 and pulsed from −90 to +80 or +100 in 10 mV steps for 4 s, then to −40 mV for 0.9 s. The interpulse interval was 15 s. G-V plots are shown in the graph to the right. The E160R-Q*Q record in red triangles in A represents only one cell responding as such at the 1 μM ML277 dose, red circles in A represent 2 cells, for all others in the figure n = 3 or 4. **(E–G)** G-V plots for E160R-Q*QQQ (E), EQQ (F), and EQ (G). Protocol as in A. **(H)** Plot of deactivation time constants (τ) versus voltage for EQ, EQQ, and EQQQQ before and after 1 μM ML277. See Table 2 for n values and statistics. Error bars throughout figure denote mean ± SEM.

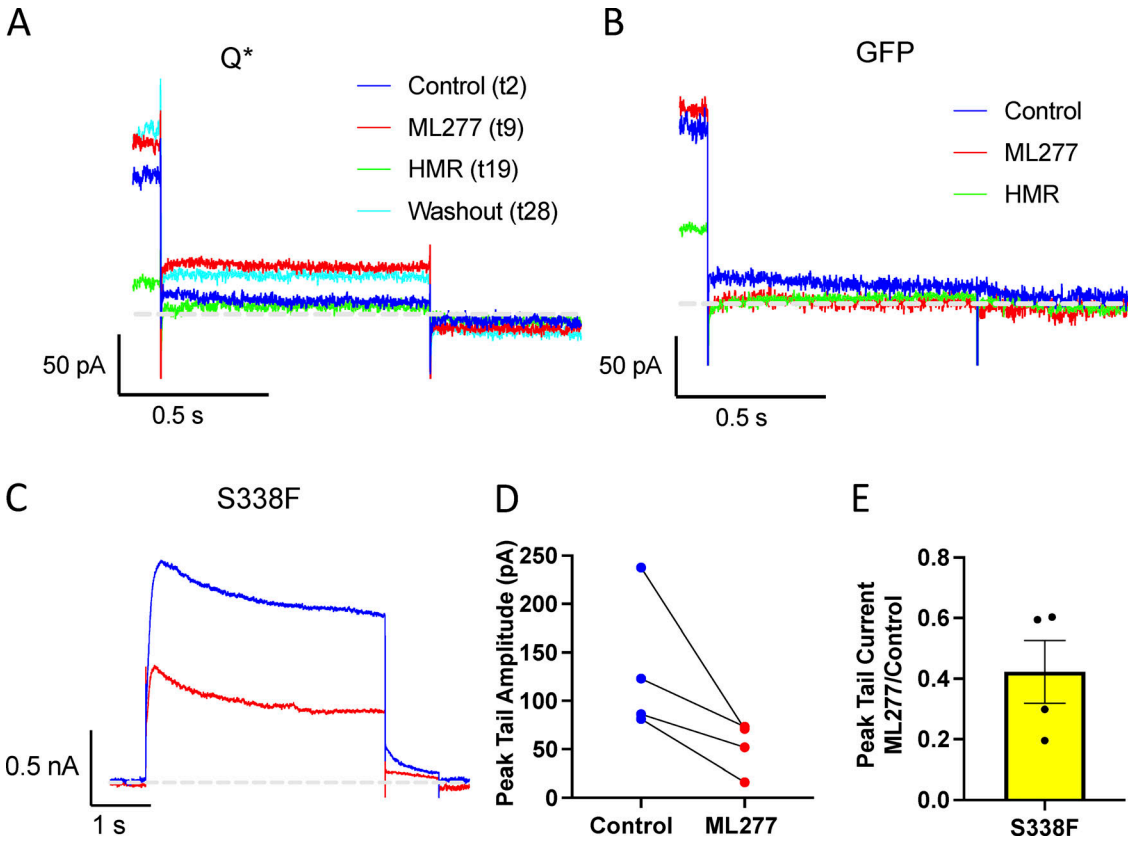

Figure S3. **HMR blocks ML277-enhanced Q* currents, and ML277 blocks the S338F mutant KCNQ1 channel. (A and B)** Tail currents from channels made up of (A) E160R-Q (Q*) and (B) GFP transfected cells, under control conditions (blue), after 1 µM ML277 (red), after 10 µM HMR + ML277 (green), and after washout (cyan). Cells were held at −80 mV, pulsed to +60 mV for 4 s, and then pulsed to −40 mV for 0.75 s. **(C)** Representative whole-cell current traces from cells before (blue trace) and after exposure to 1 µM ML277 (red trace) for KCNQ1 channel containing the S338F mutation. **(D)** Paired peak tail current measurements before and after ML277 treatment, measured after a 4-s pulse to +60 mV. **(E)** Bar chart of peak tail currents measured in ML277 divided by control peak current measurement for S338F mutant. The mean was 0.42 ± 0.10 (n = 4).